Master's thesis

NTNU
Norwegian University of Science and Technology
Faculty of Information Technology and Electrical Engineering
Department of Engineering Cybernetics

Khalil Mishal

Control Oriented Modeling of Floating Offshore Wind Turbines

Master's thesis in Industrial Cybernetics
Supervisor: Morten Dinhoff Pedersen
June 2020

NTNU
Norwegian University of Science and Technology

NTNU
Department of Engineering Cybernetics

Control Oriented Modeling of Floating Offshore Wind Turbines

Khalil Mishal

Master of Science in Engineering Cybernetics

Date: June 23, 2020
Supervisor: Associate Prof. Morten Dinhoff Pedersen, NTNU ITK

NTNU - Norwegian University of Science and Technology
Faculty of Information Technology and Electrical Engineering
Department of Engineering Cybernetics

Abstract

The energy demand in current time increases significantly, the demand rises by 1.3% each year to 2040, according to international energy agency(iea)[1]. Thus, it increases the request for a sustainable and clean energy resource such as wind energy. Wind energy technology is being exploited at significant commercial scales and established itself as a primary source for renewable energy generation. Installing wind turbines on floating platforms offshore maximizes the obtained wind power. However, locating a floating platform out into the sea carries with it some technical challenges. One significant challenge is the increased loads experienced by the turbine located on an offshore floating platform, due to the addition of waves and wind coupling to the platform's motion, etc. A number of control systems used to keep the turbine stable. The control systems' design and optimization require a reliable model that combines structural dynamics, hydrostatic, hydrodynamic, and aerodynamic loads.

In this project, a dynamic model for control applications of floating offshore wind turbines is developed. The equations of motion derived using the Newton Euler approach and formulated in a linear state space form. The model considered hydrodynamic, hydrostatic, and mooring forces for the platform and focused on deriving a new aerodynamic model mainly based on the Kutta Jouski lifting theory. Resulted model is simple to implement, where most of the calculations are predetermined in some geometrical parameters. The derived aerodynamic are represented in vectorial form, that expresses the collective and cyclic blade pitch forces in six DOF, and validated against experimental data.

Sammendrag

Dagens energibehov øker betydelig, etterspørselen øker med 1,3 % hvert år innen 2040, ifølge internasjonalt energibyrå (iea) [1]. Dermed øker det etterspørselen etter en bærekraftig og ren energiressurs som foreksempel vindenergi. Vindenergiteknologi bruk øker betydelig i kommersiell skala og etablerer seg som en primær kilde for produksjon av fornybar energi. Installering av vindturbiner på flytende offshore plattformer maksimerer den oppnådde vindkraften. Å lokalisere en flytende plattform ut i sjøen medfører noen tekniske utfordringer. En betydelig utfordring er de økte kreftene som turbinen opplever på et offshore flytende plattform på grunn av kombinasjon av bølger og vindkobling på platformen. Et antall styresystemer brukes for å holde turbinen stabil. Styresystemenes design og optimalisering krever en pålitelig modell som kombinerer strukturell dynamikk, hydrostatisk, hydrodynamisk og aerodynamisk belastning.

I dette prosjektet er det utviklet en dynamisk modell for bruk i utvikling av styringssystemer av flytende havvindturbiner. Bevegelsesligningene er utledet ved hjelp av Newton Euler tilnærmingen og formulert i en lineær tilstandsromsform. Modellen inkluderer hydrodynamiske, hydrostatiske og fortøyningskrefter for plattformen og fokuserer på å utlede en ny aerodynamisk modell hovedsakelig basert på Kutta Jouski løfteteori. Resultatmodell er enkel å implementere, der de fleste av beregningene er forhåndsbestemt i noen geometriske parametere som er utledet i dette prosjektet. Den utledede aerodynamikken er representert i vektorform, som beskriver kreftene i seks frihetsgrader, og valideres mot eksperimentelle data.

Table of Contents

List of Tables

List of Figures

Chapter 1

Introduction

1.1 Bakground

The energy demand in current time increases significantly, the demand rises by 1.3% each year to 2040, according to international energy agency(iea)[1]. Thus, it increases the request for a sustainable and clean energy resource such as wind energy. Among the renewable energy technologies, wind energy appears to be leading as a renewable alternative. Wind energy technology is being exploited at significant commercial scales and established itself as a primary source for renewable energy generation. Installing wind turbines on floating platforms far offshore, in deeper water, where the wind is stronger and steadier, maximizes the obtained wind power. Floating Offshore Wind Turbines technology is growing rapidly as the offshore wind resource has enormous potential and is advantageous in many countries with the technology solutions becoming more cost competitive.

However, locating a floating platform out into the sea carries with it some technical challenges. One significant challenge is the increased loads experienced by the turbine located on an offshore floating platform. Tower load an offshore turbine would experience increases compared to onshore wind turbines due to the addition of waves and coupling to the motion of the platform etc.

A number of control systems used to keep the turbine stable. The design and optimization of the control systems require a reliable model that combines structural dynamics, hydrostatic, hydrodynamic, and aerodynamic loads to predict the dynamic system behavior.

1.2 Assignment

The assignment is to develop a model amenable to effective control development. This model should encompass the turbine platform's motion, the gyroscopic effects due to the spinning rotor, and an effective aerodynamic model that describes the blade pitch in terms of collective and cyclic pitch. The resulted model should be presented as a linear state space model.

1.3 Modeling practice

Combining the aerodynamic, hydrodynamic, and mooring system dynamics on the floating offshore wind turbines (FOWT) creates highly complex dynamics. Methods used in modeling the fixed bottom turbines are no longer sufficient to describe the dynamics and new approaches considered for the design of the floating platform. Several models have been developed for FOWT, where most of hydrodynamic and mooring system codes and techniques are adopted from the oil and gas industry and the aerodynamic adopted from the aircraft and helicopter industry. However, those models are not readily applicable for integrated FOWT simulations[5]. Advanced numerical simulation tools such as FAST[6] and HAWC2[7] are also used. Those models give an accurate and good approximation for the physics, but unfortunately, are way too complex and not always practical for control development.

It is important to note that there is no one exact solution for the modeling problem; the best one can obtain is an approximation that is "good enough" for the purpose. This work follows the Einstein quote that says "*models should be as simple as possible but no simpler*", and aim to develop a simplified model that is accurate enough.
The model developed in this thesis finds its utility in the control development and gives an accurate description needed for individual pitch control design. The modeling process may be summarized elegantly by figure 1.1

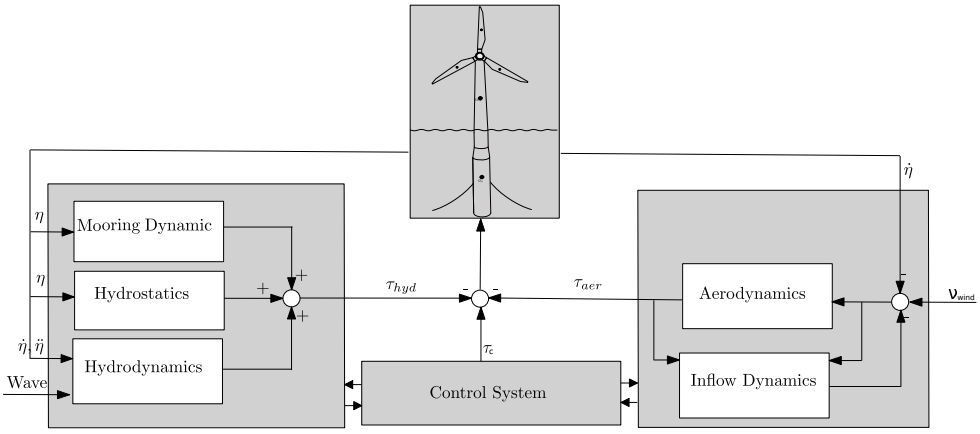

Figure 1.1: Components of the turbine modeled

1.4 Thesis outline

In chapter 2, the modeling platform kinematic and kinetics forces are presented. The tower and platform are considered as one rigid body when deriving the equations. The Newton Euler approach is used to derive the equation of motion. The system stiffens forces such as hydrostatic and mooring are presented as a linear equation. Morison equation is used here to derive the hydrodynamic force.

In chapter 3, a new model for the aerodynamic is presented. The rotor modeling includes some transformation rules based called twist and screw, and those have been defined in this chapter. Using the transformation rules together with Kutta Jouski lifting theory, an aerodynamic model, have been derived. The derived model provides an accurate estimation of the aerodynamic using collective and cyclic are validated against experimental data.

In chapter 4, the modeled systems from chapters 2 and 3 are integrated into the final model. All of the complex derivations done in the chapters before are presented in the most preferred and known form, the sate space form. The system is linearized about an operation point and described as a function of the deviation.

In chapter 5, several load cases are used to compare the modeled system against available simulation data. Systems controllability using the modeled collective and cyclic pitch model have been examined.

Chapter 2

Modeling turbine platform & hydrodynamic

In this chapter, the turbine platform and tower are modeled in six degrees of freedom, as described in table 2.1. The equation of motion is derived using the Newton Euler approach and represented in a matrix form, which allows the future implementation of the system easier. The modeling approaches and notation are based on modeling methods presented in the Fossen[2020][8]. The vectorial form in [8] seems very useful in FOWT modeling.

2.1 Platform kinematic and geometry

2.1.1 Reference frames

To derive the equation of motion of a moving body, it is convenient to define the equation relative to an inertial reference frame. Consider the platform depicted in figure 2.1, three reference frames are defined to characterize the displacement and rotation of the platform. The reference frames in this case are:

- The inertial reference frame $\{i\}$: The newton's law of motion is valid on an inertial frame, and the frame needs to be fixed. For simplicity, the inertial is defined to be coincident to body frame $\{b\}$ when the turbine is in the equilibrium position.
- The body-fixed reference frame $\{g\}$: This frame is fixed to the body with origin o_g fixed to the center of mass CM. The z axis points in the longitudinal direction through the turbine (directed from bottom to top), while the x axis points sideways to the turbine.
- The body-fixed reference frame $\{b\}$: The final equation of motion is defined in the rotor frame. This frame is fixed to the body with origin at the top of the tower with distance $\boldsymbol{r}_g^b = [0\ , 0\ , r_{g,z}]^\top$

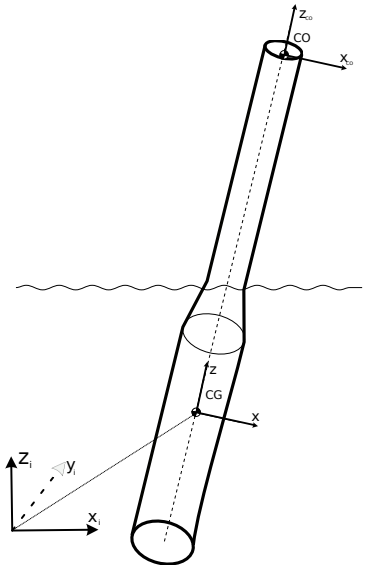

Figure 2.1: platform geometry and coordinates

2.1.2 Generalized coordinates and velocities

As mentioned earlier, the body is moving in six independent generalized coordinates. The generalized position, denoted by η, is chosen as:

$$\boldsymbol{\eta} = \begin{bmatrix} \mathbf{p}_{ib}^{i} & \Theta_{ib} \end{bmatrix}^{\top} = \begin{bmatrix} x^i & y^i & z^i & \phi & \theta & \psi \end{bmatrix}^{\top} \tag{2.1}$$

Here $\mathbf{p}_{ib}^{i}$ and Θ_{ib} are the position and angle of the body relative to inertial frame. The generalized velocities are the time derivatives of the generalized coordinates of the system:

$$\dot{\boldsymbol{\eta}} = \begin{bmatrix} \dot{\mathbf{p}}_{ib}^{i} & \dot{\Theta}_{ib} \end{bmatrix}^{\top} = \begin{bmatrix} \dot{x}^i & \dot{y}^i & \dot{z}^i & \dot{\phi} & \dot{\theta} & \dot{\psi} \end{bmatrix}^{\top} \tag{2.2}$$

Where $\dot{\mathbf{p}}_{ib}^{i}$ and $\dot{\Theta}_{ib}$ are the linear velocity and angular velocity of the body relative to inertial frame.

DOF		Body forces and moments	Body linear and angular velocities	Displacement and Euler angles
1	motions in the x-direction (surge)	f_x	u	x^n
2	motions in the y-direction (sway)	f_y	v	y^n
3	motions in the z-direction (heave)	f_z	w	z^n
4	rotation about the x-axis (roll)	m_x	p	ϕ
5	rotation about the y-axis (pitch)	m_y	q	θ
6	rotation about the z-axis (yaw)	m_z	r	ψ

Table 2.1: Platform Degrees of freedom

The angles ϕ, θ, ψ are often referred to as the Euler-Angles, also referred to as the roll, pitch, yaw-angles. The Euler angles is a rotation sequence that describe platform rotation kinematic and is commonly used for marine and flight vehicles[8]. The rotation sequence contains the three simple rotations around the x, y and z axes. These are respectively:

$$\mathbf{R}_x(\phi) = \begin{bmatrix} 1 & 0 & 0 \\ 0 & c_\phi & -s_\phi \\ 0 & s_\phi & c_\phi \end{bmatrix}, \mathbf{R}_y(\theta) = \begin{bmatrix} c_\theta & 0 & s_\theta \\ 0 & 1 & 0 \\ -s_\theta & 0 & c_\theta \end{bmatrix}, \mathbf{R}_z(\psi) = \begin{bmatrix} c_\psi & -s_\psi & 0 \\ s_\psi & c_\psi & 0 \\ 0 & 0 & 1 \end{bmatrix} \tag{2.3}$$

The corresponding rotation matrix from body to inertial frame $\mathbf{R}_{ib}$ is

$$\mathbf{R}_{ib} = \begin{bmatrix} c_\psi c_\theta & c_\psi s_\theta s_\phi - s_\psi c_\phi & c_\psi s_\theta c_\phi + s_\psi s_\phi \\ s_\psi c_\theta & s_\psi s_\theta s_\phi + c_\psi c_\phi & s_\psi s_\theta c_\phi - c_\psi s_\phi \\ -s_\theta & c_\theta s_\phi & c_\theta c_\phi \end{bmatrix}$$

where $s_{(\cdot)} = \sin_{(\cdot)}$ and $c_{(\cdot)} = \cos_{(\cdot)}$. Furthermore, it is advantageous to express the velocities in the body frame. The relationship between the velocities can be expressed as:

$$\dot{\mathbf{p}}^i_{ib} = \mathbf{R}^i_b \mathbf{v}^b_{ib} \tag{2.4}$$

for the linear velocity, and

$$\dot{\boldsymbol{\Theta}}_{nb} = \boldsymbol{T}(\boldsymbol{\Theta}_{nb})\, \omega^b_{nb} = \begin{bmatrix} 1 & \mathrm{s}_\phi \mathrm{t}_\theta & \mathrm{c}_\phi \mathrm{t}_\theta \\ 0 & \mathrm{c}_\phi & -\mathrm{s}_\phi \\ 0 & \mathrm{s}_\phi / \mathrm{c}_\theta & \mathrm{c}_\phi / \mathrm{c}_\theta \end{bmatrix} \begin{bmatrix} p \\ q \\ r \end{bmatrix} \tag{2.5}$$

for the angular velocities. The transformation is summarized in equation form in equation 2.6

$$\begin{gathered} \dot{\boldsymbol{\eta}} = \mathbf{J}_\theta(\boldsymbol{\eta})\mathbf{v} \\ \Updownarrow \\ \begin{bmatrix} \dot{\boldsymbol{p}}^n_{nb} \\ \dot{\boldsymbol{\Theta}}_{nb} \end{bmatrix} = \begin{bmatrix} \boldsymbol{R}(\boldsymbol{\Theta}_{nb}) & \mathbf{0}_{3\times3} \\ \mathbf{0}_{3\times3} & \boldsymbol{T}(\boldsymbol{\Theta}_{nb}) \end{bmatrix} \begin{bmatrix} \boldsymbol{v}^b_{nb} \\ \boldsymbol{\omega}^b_{nb} \end{bmatrix} \end{gathered} \tag{2.6}$$

2.2 Kinetics

2.2.1 Newton–Euler equations of motion

The equation of motion win turbine are derived around the center of gravity CG, using the Newton–Euler formulation. The Newton Euler equation of motion gives:

$$\frac{{}^i d}{dt} m\vec{v}_{ig} = \vec{f}_g \qquad\qquad \frac{{}^i d}{dt} I_g \vec{\omega}_{ig} = \vec{m}_g \tag{2.7}$$

Where $\vec{F}$ and $\vec{M}$ are the sum of forces and moments acting on the CG, $\boldsymbol{I}_g$ the moment of inertia about the center of gravity and $\frac{^i d}{dt}$ is the time differentiation in inertial frame $\{i\}$. Using the equation for time differentiation of a vector in rotating body frame gives the equations for the translational rotational motion:

$$\begin{aligned} \frac{^i d}{dt} m\vec{v}_{ig} &= \frac{^b d}{dt}(m\vec{v}_{ig}) + m\vec{\omega}_{ig} \times \vec{v}_{ig} \\ &= m\dot{\vec{v}}_{ig} + mS(\vec{\omega}_{ig}) \times \vec{v}_{ig} \end{aligned} \tag{2.8}$$

$$\begin{aligned} \frac{^i d}{dt} I\vec{\omega}_{ig} &= \frac{^b d}{dt}(\mathbf{I}_g\vec{\omega}_{ib}) + \vec{\omega}_{ib} \times (\mathbf{I}_g\vec{\omega}_{ib}) \\ &= \mathbf{I}_g\dot{\vec{\omega}}_{ib} - S(\mathbf{I}_g\omega_{ib})\omega_{ib} \end{aligned} \tag{2.9}$$

Where $(\cdot)$ is the skew symmetric matrix of the vector $(\cdot)$. For an arbitrary vector $\boldsymbol{a} = [a_1\ a_2\ a_3]^\top$, $\boldsymbol{S}(\boldsymbol{a})$ is expressed as

$$S(\boldsymbol{a}) = \begin{bmatrix} 0 & -a_3 & a_2 \\ a_3 & 0 & -a_1 \\ -a_2 & a_1 & 0 \end{bmatrix} \tag{2.10}$$

The skew symmetric matrix has several useful properties and simplifies cross product representation, and it is frequently used in the rest of the modeling in this report.
Summarizing the Newton–Euler equations 2.8 and 2.9, the equation can be expressed in the matrix form:

$$\mathbf{M}_{RB}\dot{\boldsymbol{\nu}} + \mathbf{C}_{RB}(\boldsymbol{\nu})\boldsymbol{\nu} = \boldsymbol{\tau} \tag{2.11}$$

$$\Updownarrow$$

$$\underbrace{\begin{bmatrix} m_t\mathbf{I}_{3\times3} & \mathbf{0}_{3\times3} \\ \mathbf{0}_{3\times3} & \mathbf{I}_g \end{bmatrix}}_{M_{RB}^{CG}} \begin{bmatrix} \dot{\mathbf{v}}_{ig}^b \\ \dot{\omega}_{ib}^b \end{bmatrix} + \underbrace{\begin{bmatrix} m_t S(\omega_{ib}^b) & \mathbf{0}_{3\times3} \\ \mathbf{0}_{3\times3} & -S(\mathbf{I}_g\omega_{ib}^b) \end{bmatrix}}_{C_{RB}^{CG}} \begin{bmatrix} \mathbf{v}_{ig}^b \\ \omega_{ib}^b \end{bmatrix} = \begin{bmatrix} \mathbf{f}_g^b \\ \mathbf{m}_g^b \end{bmatrix} \tag{2.12}$$

2.2.2 Newton–Euler equations of motion about an arbitrary origin

To simplify the further analysis of different forces formulated in different points about the body, it is desirable to derive the equation of motion for an arbitrary origin b with distance r_g^b to the center of gravity. Transformation of the forces from an arbitrary point to CG can be expressed by the simple relation:

$$\begin{aligned} \boldsymbol{f}_b^b &= \boldsymbol{f}_g^b \\ \boldsymbol{m}_b^b &= \boldsymbol{S}(r_g^b)f_b^b \end{aligned} \tag{2.13}$$

The transform of velocities can be derived as:

$$\begin{aligned}\mathbf{v}_{ig}^{b} &= \mathbf{v}_{ib}^{b} + \boldsymbol{\omega}_{ig}^{b} \times \mathbf{r}_{g}^{b} \\ &= \mathbf{v}_{ib}^{b} + S^{\top}(\mathbf{r}_{g}^{b})\boldsymbol{\omega}_{ig}^{b}\end{aligned} \tag{2.14}$$

Having established the transformation rule, the equation 2.12, will be transformed to the CO coordinate system by equation 2.15.

$$\underbrace{\mathbf{H}^{\top}(r_{g}^{b})M_{RB}^{CG}\mathbf{H}}_{M_{RB}^{CO}}\begin{bmatrix}\dot{\mathbf{v}}_{ib}^{b}\\ \dot{\omega}_{ib}^{b}\end{bmatrix} + \underbrace{\mathbf{H}^{\top}(r_{g}^{b})M_{RB}^{CG}\mathbf{H}}_{C_{RB}^{CO}}\begin{bmatrix}\mathbf{v}_{ib}^{b}\\ \omega_{ib}^{b}\end{bmatrix} = \mathbf{H}^{\top}(r_{g}^{b})\begin{bmatrix}\mathbf{f}_{g}^{b}\\ \mathbf{m}_{g}^{b}\end{bmatrix} \tag{2.15}$$

Where $\boldsymbol{H}(r_{g}^{b})$ is transformation matrix defined as:

$$\boldsymbol{H}(r_{g}^{b}) := \begin{bmatrix}\mathbf{I}_{3\times3} & S^{\top}(r_{g}^{b})\\ \mathbf{0}_{3\times3} & \mathbf{I}_{3\times3}\end{bmatrix}, \qquad \boldsymbol{H}^{\top}(r_{g}^{b}) := \begin{bmatrix}\mathbf{I}_{3\times3} & \mathbf{0}_{3\times3}\\ S(r_{g}^{b}) & \mathbf{I}_{3\times3}\end{bmatrix} \tag{2.16}$$

The matrices $\mathbf{M}_{RB}^{CO}$ and $\mathbf{C}_{RB}^{CO}$ is the mass and Coriolis matrices , m_t is the platform and tower mass and $\mathbf{I}_g$ is the inertia tensor in the center of mass.

$$\mathbf{M}_{RB}^{CO} = \begin{bmatrix}m_t\mathbf{I}_{3\times3} & -m_tS(\mathbf{r}_{g}^{b})\\ m_tS(\mathbf{r}_{g}^{b}) & \mathbf{I}_{g} - m_tS^{2}(\mathbf{r}_{g}^{b})\end{bmatrix} \tag{2.17}$$

$$\mathbf{C}_{RB}^{CO} = \begin{bmatrix}m_tS(\omega_{ib}^{b}) & -m_tS(\omega_{ib}^{b})S(\mathbf{r}_{g}^{b})\\ m_tS(\mathbf{r}_{g}^{b})S(\omega_{ib}^{b}) & -S(\mathbf{I}_{g} - m_tS^{2}(\mathbf{r}_{g}^{b}))\omega_{ib}^{b}\end{bmatrix} \tag{2.18}$$

$$\mathbf{I} = \begin{bmatrix}I_{xx} & I_{xy} & I_{xz}\\ I_{yx} & I_{yy} & I_{yz}\\ I_{zx} & I_{zy} & I_{zz}\end{bmatrix} \tag{2.19}$$

The kinetics summarized in CO frame

$$\mathbf{M}_{RB}^{CO}\dot{\boldsymbol{\nu}}^{b} + \mathbf{C}_{RB}^{CO}(\boldsymbol{\nu}^{b})\boldsymbol{\nu}^{b} = \boldsymbol{\tau}^{b} \tag{2.20}$$

2.3 Platform forces

In this section the most significant forces on the platform are modeled, this chapter is largely based on chapter 4 in [8], the same principles for ships modeling are assumed to apply for FOWT modeling. The external forces and moment considered is shown in figure2.2 those are the hydrostatic, hydrodynamic and mooring loads.

$$\tau_{RB} = \tau_{hys} + \tau_{hyd} + \tau_{mor} \tag{2.21}$$

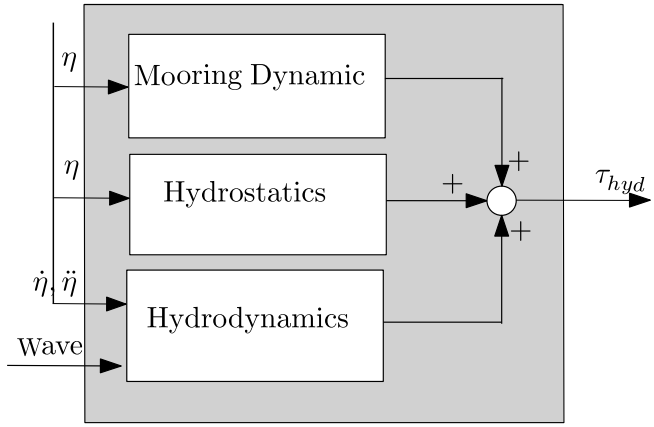

Figure 2.2: Component of hydrodynamic modeling

2.3.1 Hydrostatic forces

The hydrostatic forces considered in this derivation are the gravitational and buoyancy forces, which called restoring forces. Buoyancy is an upward force exerted by a fluid on an immersed object in a gravity field. The buoyancy force denoted by **B**, can be calculated by the Archimedes formula:

$$B = \rho g \nabla \tag{2.22}$$

For a floating platform at rest, Archimedes stated that buoyancy and weight are in balance such that:

$$mg = \rho g \nabla$$

where ∇ and z is the displaced volume and displacement in heave direction and z = 0 is the equilibrium position.

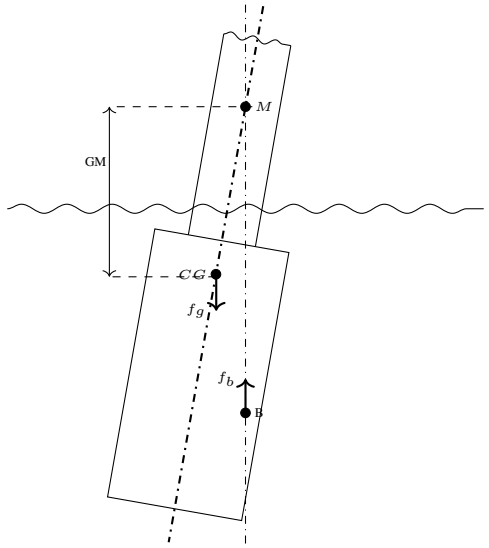

Figure 2.3: Buoyancy and gravitational force pair

The hydrostatic force in heave is the difference of the gravitational and buoyancy forces:

$$\begin{aligned} f_z &= mg\rho g(\nabla + \delta\nabla(z)) \\ &= -\rho g\delta\nabla(z) \end{aligned} \tag{2.23}$$

where $\delta\nabla(z) = \int_0^z A(\zeta)d\zeta$ is the change in displaced water, and A(ζ) is the waterplane area as a function of the heave position, $A(\zeta)$ can be assumed to be constant for small perturbations in z. The restoring hydrostatic forces are written as:

$$\mathbf{f}_{hys}^i = \begin{bmatrix} 0 \\ 0 \\ -\rho g A z \end{bmatrix} \tag{2.24}$$

in the inertial frame, which can be transformed to the body frame such that:

$$\mathbf{f}_{hys}^b = R_{ib}^\top \mathbf{f}_{hys}^i = -\rho g A z \begin{bmatrix} -sin(\theta) \\ cos(\theta)sin(\phi) \\ cos(\theta)cos(\phi) \end{bmatrix} \tag{2.25}$$

From figure 2.3, it is seen that the force pair store a moments with arms equal to -GMsin(θ) and GMsin(ϕ), where GM defined as the distance between the metacenter and center of

gravity. The restoring moment can then described as:

$$\begin{aligned} m^b_{hys} &= r^b_{GM} \times f^b_b \\ &= \begin{bmatrix} GMsin(\phi) \\ -GMsin(\theta) \\ 0 \end{bmatrix} \times -\rho g \nabla \begin{bmatrix} -sin(\theta) \\ cos(\theta)sin(\phi) \\ cos(\theta)cos(\phi) \end{bmatrix} \\ &= -\rho g \nabla \begin{bmatrix} GMsin(\phi)cos(\theta)cos(\phi) \\ GMsin(\theta)cos(\theta)cos(\phi) \\ GM(sin(\phi)sin(\theta) - cos(\theta)) \end{bmatrix} \end{aligned} \tag{2.26}$$

The restoring forces and moments can be summarized and written as:

$$\tau_{hys} = -\begin{bmatrix} \mathbf{f}^b_{hys} \\ \mathbf{m}^b_{hys} \end{bmatrix} \tag{2.27}$$

Assuming small angle pitch, and small z gives:

$$\tau_{hys} \approx \text{diag}(0, 0\rho g A, \rho g \nabla GM, \rho g \nabla GM, 0) \begin{bmatrix} x \\ y \\ z \\ \phi \\ \theta \\ \psi \end{bmatrix} \tag{2.28}$$

2.3.2 Mooring forces

The mooring is limiting the horizontal and vertical movement of the platform. For simplicity, mooring forces are modeled as linear position dependent force, as shown in figure 2.4. The mooring is modeled as a mass-spring system with components in horizontal, vertical, and yaw direction. This is shown to be a good approximation for the system stiffness.

The forces and moments equations are given by equation (2.29) about the fixing point a with distance $r^b_{moor} = [0, 0, r_z]^\top$ to the body frame CO:

$$\begin{bmatrix} f^i_{moor} \\ m^i_{moor} \end{bmatrix} = \underbrace{diag(K_x, K_y, K_z, 0, 0, K_\psi)}_{:=\mathbf{K}_{moor}} \begin{bmatrix} \mathbf{p}^i_{moor} \\ \Theta_{ib} \end{bmatrix} \tag{2.29}$$

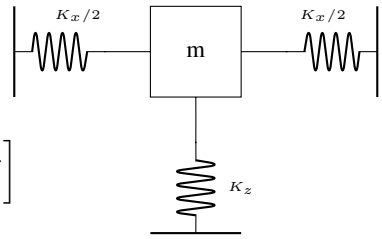

Figure 2.4: mooring mass-spring system

Since the equations of motion are derived about frame $\{b\}$, the mooring forces must be transformed into to $\{b\}$ frame. The transformation are are done by use of the transformation rule derived in section 2.2. This is shown in equation (2.30):

$$\begin{bmatrix} f_{moor}^{CO} \\ m_{moor}^{CO} \end{bmatrix} = \mathbf{H}^{\top}(r_{moor}^{b})\mathbf{K}_{moor}\mathbf{H}(r_{moor}^{b}) \begin{bmatrix} \mathbf{p}_{CO}^{i} \\ \Theta_{ib} \end{bmatrix} \tag{2.30}$$

$$\begin{bmatrix} \boldsymbol{f}_{mo}^{CO} \\ \boldsymbol{m}_{mo}^{CO} \end{bmatrix} = \begin{bmatrix} \boldsymbol{I}_{3\times3} & \mathbf{0}_{3\times3} \\ S\left(\boldsymbol{r}_{mo}\right) & \boldsymbol{I}_{3\times3} \end{bmatrix} \begin{bmatrix} diag(K_x, K_y, K_z) & \mathbf{0}_{3\times3} \\ \mathbf{0}_{3\times3} & \operatorname{diag}\left(0, 0, K_{\psi}\right) \end{bmatrix} \begin{bmatrix} \boldsymbol{I}_{3\times3} & -S\left(\boldsymbol{r}_{mo}\right) \\ \mathbf{0}_{3\times3} & \boldsymbol{I}_{3\times3} \end{bmatrix} \begin{bmatrix} \boldsymbol{p}_{CO}^{i} \\ \boldsymbol{\Theta}_{ib} \end{bmatrix}$$

$$= \begin{bmatrix} diag(K_x, K_y, K_z) & -diag(K_x, K_y, K_z)S\left(\boldsymbol{r}_{mo}\right) \\ S\left(\boldsymbol{r}_{mo}\right) diag(K_x, K_y, K_z) & -S\left(\boldsymbol{r}_{mo}\right) diag(K_x, K_y, K_z)S\left(\boldsymbol{r}_{mo}\right) + \operatorname{diag}\left(0, 0, K_{\psi}\right) \end{bmatrix} \begin{bmatrix} \boldsymbol{p}_{CO}^{i} \\ \boldsymbol{\Theta}_{ib} \end{bmatrix}$$

The system stiffness is then defined as the sum of hydrostatic and mooring forces and denoted by the matrix $\boldsymbol{G}$. The stiffens force is equal to:

$$\boldsymbol{G\eta} = \begin{bmatrix} K_x & 0 & 0 & 0 & Kr_z & 0 \\ 0 & K_y & 0 & -Kr_z & 0 & 0 \\ 0 & 0 & K_z{+}\rho g A_{wp} & 0 & 0 & 0 \\ 0 & -Kr_z & 0 & \rho g \nabla GM{-}K_x r_z^2 & 0 & 0 \\ Kr_z & 0 & 0 & 0 & \rho g \nabla GM{-}K_y r_z^2 & 0 \\ 0 & 0 & 0 & 0 & 0 & K_{\psi} \end{bmatrix} \begin{bmatrix} x \\ y \\ z \\ \phi \\ \theta \\ \psi \end{bmatrix} \tag{2.31}$$

2.3.3 Hydrodynamic forces

For the underwater structure of a floater consisting of a slender buoyant cylinder, the Morison equations can be used to evaluate the hydrodynamic loads[9]. The Morison's equation, eq. 2.32 calculate the forces resulting from the normal flow; these forces act normal to the cylindrical axis.

For this problem, the relative form of Morison's equation is utilized. This equation gives the force df_{hyd} acting on a cylindrical strip of length dz [10] the equation is shown in equation 2.32:

$$d\mathbf{f}_{hyd} = \rho\frac{\pi D^2}{4}dz\dot{\boldsymbol{\nu}}_c + \rho\frac{\pi D^2}{4}dzC_a(\dot{\boldsymbol{\nu}}_c - \dot{\boldsymbol{\nu}}) + \frac{1}{2}\rho C_d D dz(\boldsymbol{\nu}_c - \boldsymbol{\nu})|\boldsymbol{\nu}_c - \boldsymbol{\nu}| \tag{2.32}$$

Where:
D : Cylinder diameter
C_a : Added mass coefficient
C_D : Drag coefficient
$\dot{\nu}_c$: Wave acceleration at strip mid-point
ν_c : Wave velocity at mid-point

The term $\left(\frac{\pi D^2}{4} dz\right)$ is the displaced volume of fluid over time, and it's assumed to be constant. Then the total force are formulated such as :

$$\mathbf{f}_{hyd} = \underbrace{-\rho \nabla C_a \dot{\boldsymbol{\nu}}}_{\text{added mass}} + \underbrace{\rho \nabla C_m \dot{\boldsymbol{\nu}}_c}_{\text{Froude-Krylov force}} + \underbrace{\frac{1}{2} \rho A C_d \boldsymbol{\nu}_r |\boldsymbol{\nu}_r|}_{\text{Viscous Drag}} \tag{2.33}$$

Where $C_m = 1 + C_a$ is the inertia coefficient and $\boldsymbol{\nu}_r = \boldsymbol{\nu}_c - \boldsymbol{v}$ is the relative velocity. As the Morison's just considering the horizontal forces the heave force assumed to be zero, the yaw moment is also equal to zero because a cylinder is axisymmetric.

The added mass term of equation 2.33 is a function of the platform velocities and it is often shifted to the left hand side of the equation of motion,the remaining terms are function of the waves dynamic, it will be denoted as τ_{hyd^*}. The added mass is then formulated in matrix for and transformed to CO frame where the equation of motion defined:

$$\begin{bmatrix} \boldsymbol{I}_{3\times3} & \boldsymbol{0}_{3\times3} \\ S(\boldsymbol{r}_{hyd}) & \boldsymbol{I}_{3\times3} \end{bmatrix} \begin{bmatrix} \text{diag}(-\rho\nabla C_a, -\rho\nabla C_a, 0) & 0_{3\times3} \\ 0_{3\times3} & 0_{3\times3} \end{bmatrix} \begin{bmatrix} \boldsymbol{I}_{3\times3} & -S(\boldsymbol{r}_{hyd}) \\ \boldsymbol{0}_{3\times3} & \boldsymbol{I}_{3\times3} \end{bmatrix} \tag{2.34}$$

The added matrix at the CO frame is then defined as:

$$\begin{bmatrix} A_{11} & 0 & 0 & 0 & A_{15} & 0 \\ & A_{22} & 0 & A_{24} & 0 & 0 \\ & & 0 & 0 & 0 & 0 \\ & sym & & A_{44} & 0 & 0 \\ & & & & A_{55} & 0 \\ & & & & & 0 \end{bmatrix} \tag{2.35}$$

The elements of the added mass matrix are

$$A_{11} = A_{22} = \rho \nabla C_a \quad A_{15} = -A_{24} = A_{11} r_{hyd} \quad , \quad A_{44} = A_{55} = A_{11} r_{hyd}^2$$

Chapter summary:
Summarizing all force derived in this chapter, the equation of motion is:

$$(\boldsymbol{M} + \boldsymbol{A})\dot{\boldsymbol{\nu}} + \boldsymbol{C}\boldsymbol{\nu} + \boldsymbol{G}\boldsymbol{\eta} = \boldsymbol{\tau}_{hyd*} \tag{2.36}$$

Chapter 3

Modeling turbine rotor & aerodynamic

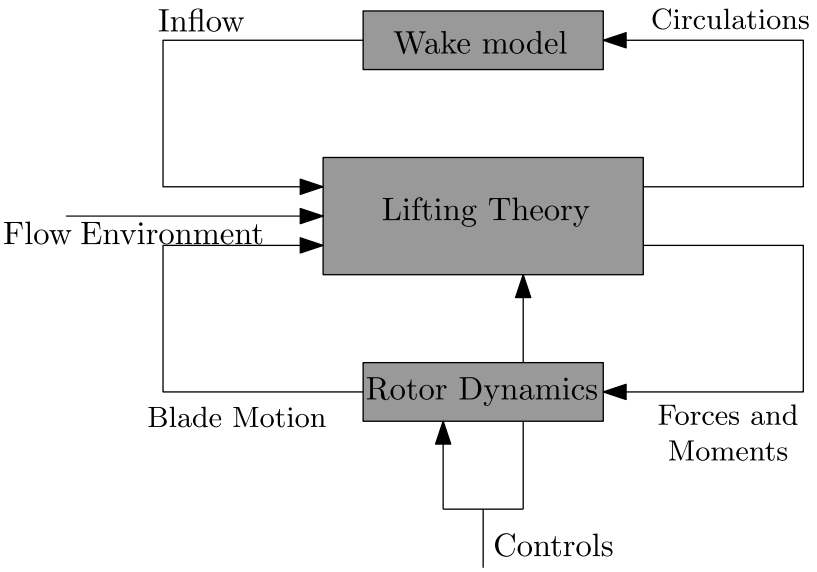

Figure 3.1: Components of the rotor model [4]

In this chapter, an accurate model for the rotor and aerodynamic load is developed. The rotor modeling is summarized elegantly in figure3.1. Unlike most of the developed models, the developed model is not based on the blade element theory (BEM). The model in this chapter is based on the Jouwski rotor and vectorial vortex theory. However, this model will be validated against BEM developed codes.

3.1 Rotor kinematic

Rotor modeling include some complex derivations and transformations; thus, it is important to have the transformation rules established.

3.1.1 Twists and screws

A twist is a generalized velocity containing both translational and rotational velocity. We shall denote such objects by

$$\boldsymbol{v} = \begin{bmatrix} v \\ \omega \end{bmatrix} \tag{3.1}$$

Twists are used to generate a vector field using six parameter such as:

$$v(x) = \begin{bmatrix} I & -S(x) \end{bmatrix} \boldsymbol{v} \tag{3.2}$$

Screws are generalized forces that contain both force and torque. This type of object will be denoted by

$$\boldsymbol{\tau} = \begin{bmatrix} f \\ m \end{bmatrix} \tag{3.3}$$

Screws use a vector field to generate six parameters by

$$\boldsymbol{\tau} = \int \begin{bmatrix} I \\ S(x) \end{bmatrix} f(x) dx \tag{3.4}$$

Without going in detail of derivation, two important transformation rules are used here. The transformation matrix for twists and screws in two reference frames are defined as:

$$\boldsymbol{v}' = \boldsymbol{T}\boldsymbol{v}, \quad \boldsymbol{T} \triangleq \begin{bmatrix} R & S(r)R \\ 0 & R \end{bmatrix}, \boldsymbol{\tau} = \tilde{\boldsymbol{T}}\boldsymbol{\tau}', \quad \tilde{\boldsymbol{T}} \triangleq \begin{bmatrix} R & 0 \\ S(r)R & R \end{bmatrix} \tag{3.5}$$

Twists are dual to screws in the following sense:

$$\boldsymbol{v}^\top \boldsymbol{\tau} = (\boldsymbol{T}\boldsymbol{v}')^\top \left(\tilde{\boldsymbol{T}}\boldsymbol{\tau}'\right) = \boldsymbol{v}'^\top \boldsymbol{T}^\top \tilde{\boldsymbol{T}} \boldsymbol{\tau}' = \boldsymbol{v}'^\top \boldsymbol{\tau}' \tag{3.6}$$

These results show to be very useful when transforming the wind vector fields between the frames. The results of screw and twist include several mathematical steps discussed in [11].

3.1.2 Reference frames

For rotor modeling, three different Reference frames are used.

- Inertial frame denoted $\{\mathrm{I}\}$
- Rotor frame denoted $\{\mathrm{r}\}$
- Blade frames denoted $\{b_i\}$ for each blade

Rotation between frames is described by Euler angles in a similar approach used for the platform kinematic.

3.1.3 Flow representation

The flow model used for deviation of the aerodynamic forces is the relative velocity of the rotor. The flow is composed of:

- External wind and wind shear flow $\boldsymbol{\nu}_0$
- Wake induced flow $\boldsymbol{\nu}_i$
- Flow from the platform and rotor motion $\boldsymbol{\nu}$

The relative flow vector denoted $\boldsymbol{\mu}$ can then be expressed such that:

$$\boldsymbol{\mu} = \boldsymbol{\nu}_0 - \boldsymbol{\nu}_i - \boldsymbol{\nu} \tag{3.7}$$

Here $\boldsymbol{\mu}$ is the 6x6 velocity twist that describes relative flow on rotor frame. The relative flow will be transformed into a 3×3 matrix in the blade frame. The forces are found in the blade frame after that transformed back to the rotor frame. The transformation of velocities and forces can be elegantly summarized by figure 3.2. These transformations give us a simple representation of forces in 6 degrees of freedom.

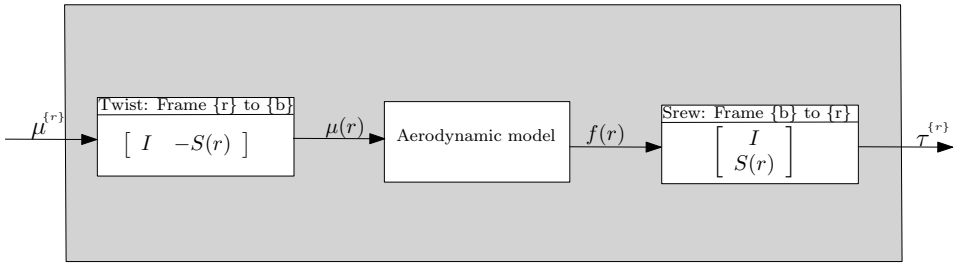

Figure 3.2: Caption

3.2 Aerodynamic forces

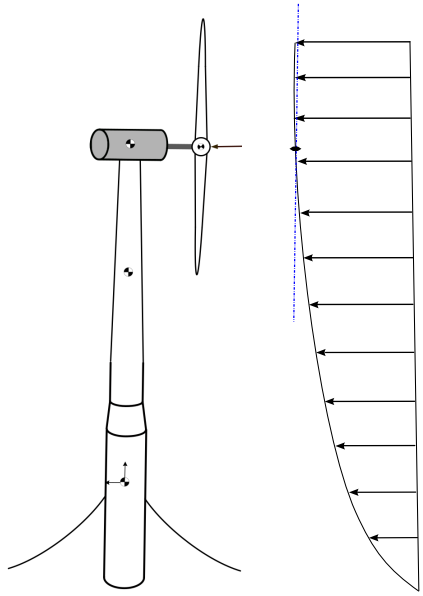

Figure 3.3: Caption

3.2.1 Kutta–Joukowski relation

The airflow impacts the rotor blades and induces friction on them, which produces an aerodynamic force. The force is decomposed into two components called the lift and drag forces, perpendicular and parallel to the inflow, respectively. The vorticity carried by the airfoil is responsible for the lift force, and the Kutta–Joukowski theorem gives the relation between the airfoil circulation and the steady lift force[12], by equation

$$f_{\text{lift}}(x) = \rho\gamma(x) \times \mu(x) \tag{3.8}$$

3.2.2 Geometric blade element method

In this section, the aerodynamic forces on a straight lifting line are considered. Consider Figure 3.5, which shows a coordinate system attached at the root of a blade. The coordinates in this frame will be denoted by x = col(x, r, z) and denote the position along t, l, and n, respectively. Airfoil sections with a twist θ(r) and chord length c(r) are placed along the lifting line.

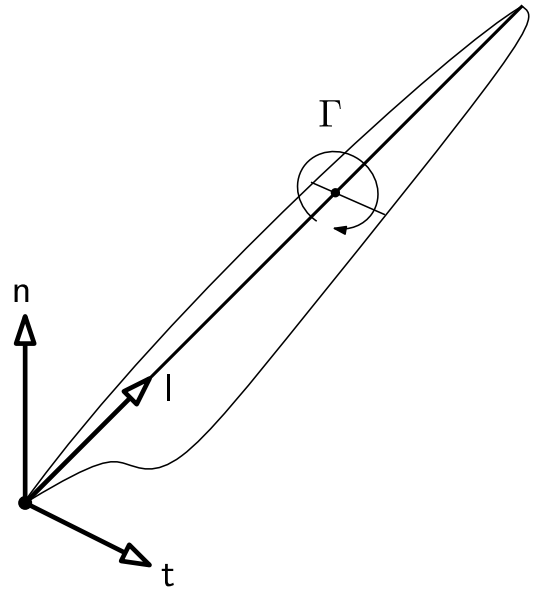

Figure 3.4: The coordinate system of the blade

Lift forces
The vectorial Kutta–Joukowski theorem informs us that lift is given by the relation

$$f_{\text{lift}}(x) = \rho S(\gamma(x))\mu(x) \tag{3.9}$$

Here, ρ is the air density, γ the vorticity and μ the relative flow. The lifting line approximation concentrates all vorticity along a lifting line, therefore

$$\gamma(x) = e_l \Gamma(r) \tag{3.10}$$

where $e_l = [0, 1, 0]^\top$. This implies the concentrated lift distribution given by

$$f_{\text{lift}}(x) = \rho \Gamma(r) S(e_l)\, \mu(x) \tag{3.11}$$

Drag forces
Drag can be modeled in an analogous manner with the following formula

$$f_{\text{drag}}(x) = \rho \delta(r) \left(I - e_l e_l^\top\right) \mu(x) \tag{3.12}$$

Here, $\delta(r)$ serves as a coefficient in a drag formula following Hoerner's crossflow-principle. We shall let

$$\delta(r) = dc(r)|\mu(x)| \tag{3.13}$$

where d is constant. This choice implies the following energy dissipation due to drag.

$$\mu(x)^\top f_{\text{drag}}(x) = \rho dc(r)|\mu(x)|\mu(x)^\top \left(I - e_l e_l^\top\right) \mu(x) \tag{3.14}$$

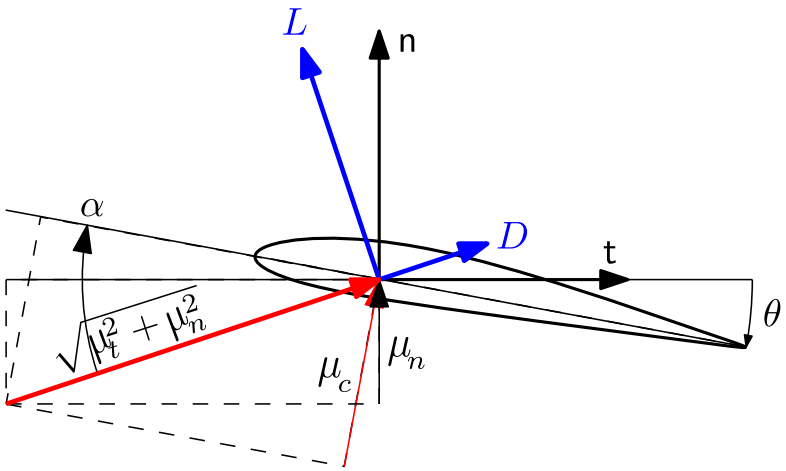

Figure 3.5: The blade 2D section and velocity definition

The forces for lift and drag derived in equations 3.11 and 3.12 are the the forces on the 2D section as shown in figure 3.5. The complete force for the blade are obtained by integrating over the blade length.

Integration of lift
One can integrate over the lift expression to arrive at a screw which accounts for all forces and torques on the blade.

$$\boldsymbol{\tau}_{\text{lift}} = \rho \int_0^R \begin{bmatrix} I \\ S(e_l r) \end{bmatrix} \Gamma(r) S(e_l) \mu(r)\, dr \tag{3.15}$$

We shall assume that the relative flow can be captured by a twist employed via the following expression.

$$\mu(x) = \begin{bmatrix} I & -S(x) \end{bmatrix} \boldsymbol{\mu} \tag{3.16}$$

Thus, the lift force in blade frame are formulated as

$$\boldsymbol{\tau}_{\text{lift}} = \rho \left(\int_0^R \begin{bmatrix} I \\ S(e_l r) \end{bmatrix} S(e_l) \begin{bmatrix} I & -S(e_l r) \end{bmatrix} \Gamma(r)\, dr \right) \boldsymbol{\mu} \tag{3.17}$$

This is a linear relationship which may be written as

$$\boldsymbol{\tau}_{\text{lift}} = \boldsymbol{\Lambda} \boldsymbol{\mu} \tag{3.18}$$

Employing the identity $S^2(v) = vv^\top - \left(v^\top v\right) I$, the integrals in the lift matrix may be taken in the following fashion.

$$\mathbf{\Lambda} \triangleq \rho \int_0^R \begin{bmatrix} \Gamma(r)S(e_l) & -\Gamma(r)rS^2(e_l) \\ \Gamma(r)rS^2(e_l) & -\Gamma(r)r^2S^3(e_l) \end{bmatrix} dr = \rho \begin{bmatrix} g_0 S(e_l) & -g_1 S^2(e_l) \\ g_1 S^2(e_l) & -g_2 S^3(e_l) \end{bmatrix} \tag{3.19}$$

The following integrals were defined, and referred to as circulation parameters.

$$g_0 \triangleq \int_0^R \Gamma(r)\, dr, \qquad g_1 \triangleq \int_0^R \Gamma(r) r\, dr, \qquad g_2 \triangleq \int_0^R \Gamma(r) r^2\, dr \tag{3.20}$$

Circulation is determined by the flow perpendicular to the airfoil μ_c and is proportional to the airfoil chord length. Let $e_n = [1, 0, 0]^\top$. The normal crossflow at a blade twisted with the angle θ is given by

$$\begin{aligned} \Gamma(r) &= \pi c(r) \mu_c(r) && (3.21)\\ &= \pi c(r) (R(\theta(r)) e_n)^\top \begin{bmatrix} I & -S(e_l r) \end{bmatrix} \boldsymbol{\mu} && (3.22)\\ &= \pi c(r) \begin{bmatrix} \cos(\theta) & 0 & -\sin(\theta) & -r\sin(\theta) & 0 & -r\cos(\theta) \end{bmatrix} \boldsymbol{\mu} && (3.23) \end{aligned}$$

$$s_0 \triangleq \int_0^R \pi c(r) \sin(\theta(r))\, dr \tag{3.24}$$

$$c_0 \triangleq \int_0^R \pi c(r) \cos(\theta(r))\, dr \tag{3.25}$$

$$s_1 \triangleq \int_0^R \pi r c(r) \sin(\theta(r))\, dr \tag{3.26}$$

$$c_1 \triangleq \int_0^R \pi r c(r) \cos(\theta(r))\, dr \tag{3.27}$$

$$s_2 \triangleq \int_0^R \pi r^2 c(r) \sin(\theta(r))\, dr \tag{3.28}$$

$$c_2 \triangleq \int_0^R \pi c r^2(r) \cos(\theta(r))\, dr \tag{3.29}$$

$$s_3 \triangleq \int_0^R \pi r^3 c(r) \sin(\theta(r))\, dr \tag{3.30}$$

$$c_3 \triangleq \int_0^R \pi r^3 c(r) \cos(\theta(r))\, dr \tag{3.31}$$

$$\tag{3.32}$$

These parameters are referred to as the geometrical lifting parameters.

$$\boldsymbol{\kappa}_0 \triangleq \begin{bmatrix} c_0 \\ 0 \\ -s_0 \\ -s_1 \\ 0 \\ -c_1 \end{bmatrix}, \quad \boldsymbol{\kappa}_1 \triangleq \begin{bmatrix} c_1 \\ 0 \\ -s_1 \\ -s_2 \\ 0 \\ -c_2 \end{bmatrix}, \quad \boldsymbol{\kappa}_2 \triangleq \begin{bmatrix} c_2 \\ 0 \\ -s_2 \\ -s_3 \\ 0 \\ -c_3 \end{bmatrix} \tag{3.33}$$

$$g_0 = \boldsymbol{\kappa}_0^\top \boldsymbol{\mu},\ g_1 = \boldsymbol{\kappa}_1^\top \boldsymbol{\mu},\ g_2 = \boldsymbol{\kappa}_2^\top \boldsymbol{\mu}, \tag{3.34}$$

This leads to the final expression for the forces on a single blade, as measured in the blade frame.

$$\boldsymbol{\tau}_{\text{lift}} = \boldsymbol{\Lambda}(1,4)\boldsymbol{\mu}, \quad \boldsymbol{\Lambda}(\boldsymbol{\mu}) = \rho \begin{bmatrix} (\boldsymbol{\kappa}_0^\top \boldsymbol{\mu}) S(e_l) & -(\boldsymbol{\kappa}_1^\top \boldsymbol{\mu}) S^2(e_l) \\ (\boldsymbol{\kappa}_1^\top \boldsymbol{\mu}) S^2(e_l) & -(\boldsymbol{\kappa}_2^\top \boldsymbol{\mu}) S^3(e_l) \end{bmatrix} \tag{3.35}$$

Integration of drag:

$$\begin{aligned} \boldsymbol{\tau}_{\text{drag}} &= \rho \int_0^R \begin{bmatrix} I \\ S(e_l r) \end{bmatrix} \delta(r) \left(I - e_l e_l^\top\right) \mu(r) dr \\ &= \rho \left(\int_0^R \begin{bmatrix} I \\ S(e_l r) \end{bmatrix} \left(I - e_l e_l^\top\right) \begin{bmatrix} I & -S(e_l r) \end{bmatrix} \delta(r) dr \right) \boldsymbol{\mu} \end{aligned} \tag{3.36}$$

Now let

$$\boldsymbol{\tau}_{\text{drag}} = \boldsymbol{\Delta}\boldsymbol{\mu} \tag{3.37}$$

where

$$\boldsymbol{\Delta} \triangleq \rho \int_0^R \begin{bmatrix} -\delta(r) S^2(e_l) & -\delta(r) r S(e_l) \\ \delta(r) r S(e_l) & -\delta(r) r^2 S^2(e_l) \end{bmatrix} dr = \rho \begin{bmatrix} -a_0 S^2(e_l) & -a_1 S(e_l) \\ a_1 S(e_l) & -a_2 S^2(e_l) \end{bmatrix} \tag{3.38}$$

Here,

$$a_0 \triangleq \int_0^R \delta(r) dr, \quad a_1 \triangleq \int_0^R \delta(r) r dr, \quad a_2 \triangleq \int_0^R \delta(r) r^2 dr \tag{3.39}$$

Now, $\delta(r) = dc(r)|\mu(x)|$ which implies that

$$\delta(r) = dc(r) \sqrt{\boldsymbol{\mu}^\top \begin{bmatrix} I & -rS(e_l) \\ rS(e_l) & rS^2(e_l) \end{bmatrix} \boldsymbol{\mu}} \tag{3.40}$$

Let a normalized twist be introduced with

$$\tilde{\boldsymbol{\mu}} \triangleq \begin{bmatrix} v \\ \omega R \end{bmatrix} \tag{3.41}$$

This quantity puts velocities and rotation-rates on equal footing and makes for a reasonable inner product. A conservative estimate for the (positive) drag coefficient may be obtained via the following device.

$$0 \leq \tilde{\mu}^\top \begin{bmatrix} I & -(r/R)S(e_l) \\ (r/R)S(e_l) & (r/R)^2 S^2(e_l) \end{bmatrix} \tilde{\mu} \leq \lambda_{\max}\left(\begin{bmatrix} I & -rS(e_l) \\ rS(e_l) & (r/R)^2 S^2(e_l) \end{bmatrix} \right) \tilde{\boldsymbol{\mu}}^\top \tilde{\boldsymbol{\mu}}$$
$$= \left(1 + \left(\frac{r}{R}\right)^2\right) |\tilde{\boldsymbol{\mu}}|^2 \quad (3.42)$$

It follows that

$$\delta(r) \leq dc(r)\sqrt{1 + \left(\frac{r}{R}\right)^2}|\tilde{\boldsymbol{\mu}}| \quad (3.43)$$

Hence,

$$a_0 = d|\tilde{\boldsymbol{\mu}}| \int_0^R c(r)\sqrt{1 + \left(\frac{r}{R}\right)^2} dr \quad (3.44)$$

$$a_1 = d|\tilde{\boldsymbol{\mu}}| \int_0^R c(r) r \sqrt{1 + \left(\frac{r}{R}\right)^2} dr \quad (3.45)$$

$$a_2 = d|\tilde{\boldsymbol{\mu}}| \int_0^R c(r) r^2 \sqrt{1 + \left(\frac{r}{R}\right)^2} dr \quad (3.46)$$

Individual Pitch
Before transforming the forces to the rotor frame, the concept of individual pitch has to be presented. The pitch angle α may vary between when using the individual pitch control, a common way to express the individual pitch on the blades is through cyclic pitch. Cyclic pitch control is well represented in the field of helicopter control[13]. The pitch angle for each blade will be presented as

$$\alpha_i = \alpha_0 + \alpha_c \cos(\phi) + \alpha_s \sin(\phi) \quad (3.47)$$

where the angle α_0 is the collective pitch, while α_c and α_s are the cyclic pitch. The collective pitch is the averaged pitch for which is the same for all the blades and control the total thrust on the rotor, while the cyclic pitch angles are a function of the rotor azimuth angle and control the flap moment about the rotor plane.

3.2.3 Transformation to rotor frame

We now proceed to assemble several identical blades to produce a rotor. In the blade's local frame it holds that

$$\boldsymbol{\tau}'_{\text{lift}} = \boldsymbol{\Lambda}(\boldsymbol{\mu}')\,\boldsymbol{\mu}' \quad (3.48)$$

Consider now a fixed frame about which the blade may rotate. The coordinate transformation from the checked blade frame to the stationary frame is given by $x = Rx'$ where

$$R(\phi, \alpha) = \begin{bmatrix} 1 & 0 & 0 \\ 0 & \cos(\phi) & -\sin(\phi) \\ 0 & \sin(\phi) & \cos(\phi) \end{bmatrix} = \begin{bmatrix} \cos(\alpha) & 0 & \sin(\alpha) \\ 0 & 1 & 0 \\ -\sin(\alpha) & 0 & \cos(\alpha) \end{bmatrix}$$

By replacing the pitch angle α by collective and cyclic angles in equation3.47, the transformation is then fully determined by ϕ, and one may write

$$R(\phi) = \begin{bmatrix} \cos(\alpha) & 0 & \sin(\alpha) \\ 0 & 1 & 0 \\ -\sin(\alpha) & 0 & \cos(\alpha) \end{bmatrix}$$
$$\begin{bmatrix} cos(\alpha_0 + \alpha_c cos(\phi) + \alpha_s sin(\phi)) & 0 & sin(\alpha_0 + \alpha_c cos(\phi) + \alpha_s sin(\phi)) \\ 0 & 1 & 0 \\ -sin(\alpha_0 + \alpha_c cos(\phi) + \alpha_s sin(\phi)) & 0 & cos(\alpha_0 + \alpha_c cos(\phi) + \alpha_s sin(\phi)) \end{bmatrix} \tag{3.49}$$

Since there is no frame offset, the twist and screw transformation matrices reduce to

$$\mathbf{T}(\phi) = \tilde{\mathbf{T}} = \begin{bmatrix} R(\phi) & 0 \\ 0 & R(\phi) \end{bmatrix} \tag{3.50}$$

Using the transformation rules derived in section 3.1, the lift and forces for single blade in the rotor frame are expressed by

$$\boldsymbol{\tau}_{\text{lift}} = \tilde{\mathbf{T}}\boldsymbol{\Lambda}(\mathbf{q}')\mathbf{q}' = \tilde{\mathbf{T}}\boldsymbol{\Lambda}(\mathbf{T}^{-1}\boldsymbol{\mu})\mathbf{T}^{-1}\boldsymbol{\mu} \tag{3.51}$$
$$\boldsymbol{\tau}_{\text{drag}} = \tilde{\mathbf{T}}\boldsymbol{\Delta}\mathbf{T}^{-1}\boldsymbol{\mu} \tag{3.52}$$

One may proceed by averaging the contribution from each blade over one cycle of rotation, yielding the force

$$\boldsymbol{\tau}_{\text{lift}} = \left(\frac{1}{2\pi}\int_0^{2\pi} (\tilde{\mathbf{T}}(\phi)\boldsymbol{\Lambda}(\mathbf{T}^{-1}(\phi)\boldsymbol{\mu})\mathbf{T}^{-1}(\phi)\right)\boldsymbol{\mu} \tag{3.53}$$

$$\boldsymbol{\tau}_{\text{drag}} = \left(\frac{1}{2\pi}\int_0^{2\pi} (\tilde{\mathbf{T}}(\phi)\boldsymbol{\Delta}\mathbf{T}^{-1}(\phi)\right)\boldsymbol{\mu} \tag{3.54}$$

Multiplying this expression with the number of blades yields, the final expression for the forces are

$$\boldsymbol{\tau}_{\text{lift}} \approx B\left[\bar{\boldsymbol{\Lambda}}(\boldsymbol{\mu}) + \alpha_0\boldsymbol{\Lambda}_0(\boldsymbol{\mu}) + \alpha_c\boldsymbol{\Lambda}_c(\boldsymbol{\mu}) + \alpha_s\boldsymbol{\Lambda}_s(\boldsymbol{\mu})\right]\boldsymbol{\mu} \tag{3.55}$$

$$\boldsymbol{\tau}_{\text{drag}} \approx B\bar{\boldsymbol{\Delta}}\boldsymbol{\mu} \tag{3.56}$$

Here the B is the number of blades. In this expression, the pitch angle is assumed small, and the small angle approximation is used here.

The matrices in equation 3.55 and 3.56 are. defined as

$$\bar{\mathbf{\Lambda}}(\boldsymbol{\mu}) = \begin{bmatrix} 0 & \frac{1}{2}(c_1(-\mu_5)-\mu_2 s_0) & \frac{1}{2}(c_1(-\mu_6)-\mu_3 s_0) & c_1\mu_1-\mu_4 s_2 & 0 & 0 \\ \frac{1}{2}(c_1\mu_5+\mu_2 s_0) & 0 & 0 & 0 & \frac{1}{2}(c_1\mu_1-\mu_4 s_2) & 0 \\ \frac{1}{2}(c_1\mu_6+\mu_3 s_0) & 0 & 0 & 0 & 0 & \frac{1}{2}(c_1\mu_1-\mu_4 s_2) \\ \mu_4 s_2-c_1\mu_1 & 0 & 0 & 0 & \frac{1}{2}(c_3(-\mu_5)-\mu_2 s_2) & \frac{1}{2}(c_3(-\mu_6)-\mu_3 s_2) \\ 0 & \frac{1}{2}(\mu_4 s_2-c_1\mu_1) & 0 & \frac{1}{2}(c_3\mu_5+\mu_2 s_2) & 0 & 0 \\ 0 & 0 & \frac{1}{2}(\mu_4 s_2-c_1\mu_1) & \frac{1}{2}(c_3\mu_6+\mu_3 s_2) & 0 & 0 \end{bmatrix} \tag{3.57}$$

$$\mathbf{\Lambda}_0(\boldsymbol{\mu}) = \begin{bmatrix} 0 & \frac{1}{2}(\mu_5 s_1-c_0\mu_2) & \frac{1}{2}(\mu_6 s_1-c_0\mu_3) & c_2(-\mu_4)-\mu_1 s_1 & 0 & 0 \\ \frac{1}{2}(c_0\mu_2-\mu_5 s_1) & 0 & 0 & 0 & \frac{1}{2}(c_2(-\mu_4)-\mu_1 s_1) & 0 \\ \frac{1}{2}(c_0\mu_3-\mu_6 s_1) & 0 & 0 & 0 & 0 & \frac{1}{2}(c_2(-\mu_4)-\mu_1 s_1) \\ c_2\mu_4+\mu_1 s_1 & 0 & 0 & 0 & \frac{1}{2}(\mu_5 S_3-c_2\mu_2) & \frac{1}{2}(\mu_6 S_3-c_2\mu_3) \\ 0 & \frac{1}{2}(c_2\mu_4+\mu_1 s_1) & 0 & \frac{1}{2}(c_2\mu_2-\mu_5 S_3) & 0 & 0 \\ 0 & 0 & \frac{1}{2}(c_2\mu_4+\mu_1 s_1) & \frac{1}{2}(c_2\mu_3-\mu_6 S_3) & 0 & 0 \end{bmatrix} \tag{3.58}$$

$$\mathbf{\Lambda}_c(\boldsymbol{\mu}) = \begin{bmatrix} 0 & 0 & \frac{1}{2}(c_1(-\mu_4)-\mu_1 s_0) & \frac{1}{2}(\mu_6 s_2-c_1\mu_3) & 0 & 0 \\ 0 & 0 & 0 & 0 & \frac{1}{8}(\mu_6 s_2-c_1\mu_3) & \frac{1}{8}(\mu_5 s_2-c_1\mu_2) \\ \frac{1}{2}(c_1\mu_4+\mu_1 s_0) & 0 & 0 & 0 & \frac{1}{8}(\mu_5 s_2-c_1\mu_2) & \frac{3}{8}(\mu_6 s_2-c_1\mu_3) \\ \frac{1}{2}(c_1\mu_3-\mu_6 s_2) & 0 & 0 & 0 & 0 & \frac{1}{2}(c_3(-\mu_4)-\mu_1 s_2) \\ 0 & \frac{1}{8}(c_1\mu_3-\mu_6 s_2) & \frac{1}{8}(c_1\mu_2-\mu_5 s_2) & 0 & 0 & 0 \\ 0 & \frac{1}{8}(c_1\mu_2-\mu_5 s_2) & \frac{3}{8}(c_1\mu_3-\mu_6 s_2) & \frac{1}{2}(c_3\mu_4+\mu_1 s_2) & 0 & 0 \end{bmatrix} \tag{3.59}$$

$$\mathbf{\Lambda}_s(\boldsymbol{\mu}) = \begin{bmatrix} 0 & \frac{1}{2}(c_1\mu_4+\mu_1 s_0) & 0 & \frac{1}{2}(c_1\mu_2-\mu_5 s_2) & 0 & 0 \\ \frac{1}{2}(c_1(-\mu_4)-\mu_1 s_0) & 0 & 0 & 0 & \frac{3}{8}(c_1\mu_2-\mu_5 s_2) & \frac{1}{8}(c_1\mu_3-\mu_6 s_2) \\ 0 & 0 & 0 & 0 & \frac{1}{8}(c_1\mu_3-\mu_6 s_2) & \frac{1}{8}(c_1\mu_2-\mu_5 s_2) \\ \frac{1}{2}(\mu_5 s_2-c_1\mu_2) & 0 & 0 & 0 & \frac{1}{2}(c_3\mu_4+\mu_1 s_2) & 0 \\ 0 & \frac{3}{8}(\mu_5 s_2-c_1\mu_2) & \frac{1}{8}(\mu_6 s_2-c_1\mu_3) & \frac{1}{2}(c_3(-\mu_4)-\mu_1 s_2) & 0 & 0 \\ 0 & \frac{1}{8}(\mu_6 s_2-c_1\mu_3) & \frac{1}{8}(\mu_5 s_2-c_1\mu_2) & 0 & 0 & 0 \end{bmatrix} \tag{3.60}$$

$$\bar{\mathbf{\Delta}} = \begin{bmatrix} a_0 & 0 & 0 & 0 & 0 & 0 \\ 0 & \frac{a_0}{2} & 0 & 0 & 0 & 0 \\ 0 & 0 & \frac{a_0}{2} & 0 & 0 & 0 \\ 0 & 0 & 0 & a_2 & 0 & 0 \\ 0 & 0 & 0 & 0 & \frac{a_2}{2} & 0 \\ 0 & 0 & 0 & 0 & 0 & \frac{a_2}{2} \end{bmatrix} \boldsymbol{\mu} \tag{3.61}$$

3.2.4 Induced velocity

The dynamic inflow model that are used to determine the wake induced velocity are proposed by Pedersen in [2]. Through a set of concepts and mathematical theories, a dynamic inflow model describing the averaged inflow are being represented by convolution [2].

$$\boldsymbol{\nu}_i(t) = \int_0^t G\left(t, t'\right) F\left(t'\right) dt' \qquad \text{(Dynamic inflow relation)}$$

$$G\left(t, t'\right) \triangleq \frac{\Theta\left(t - t'\right)}{\rho A} \int_0^\infty J_1(lR)^2 e^{-l\left|z\left(t,t'\right)\right|} dl \qquad \text{(Vortical impulse response)}$$

The theory presented is derived based on conservation of momentum and vortex ring consideration. It is shown that thee theory is equal to the Rankine-Froude momentum theory at steady state response [2]. Through a frequency domain exploration the presented dynamic wake model was realized as a nonlinear ODE. It is also derived a first order model with low frequency limit of the general theory, the low frequency approximation will be useful for this work. Equation 3.62 shows the final model with a low frequency approximation that is used in the further analysis in this project.

$$2\rho A R \mu v_i(t) + 2\rho A |v| v_i(t) = F(t) \tag{3.62}$$

$$\mu \triangleq \frac{8}{3\pi}$$

Hhere μ plays the role of a dimensionless "virtual inertia". The model can be compared to other existing models such as Øye's vortex model, and it is shown in figure 3.6 that the model 3.62 compares well to the Øye model.

s

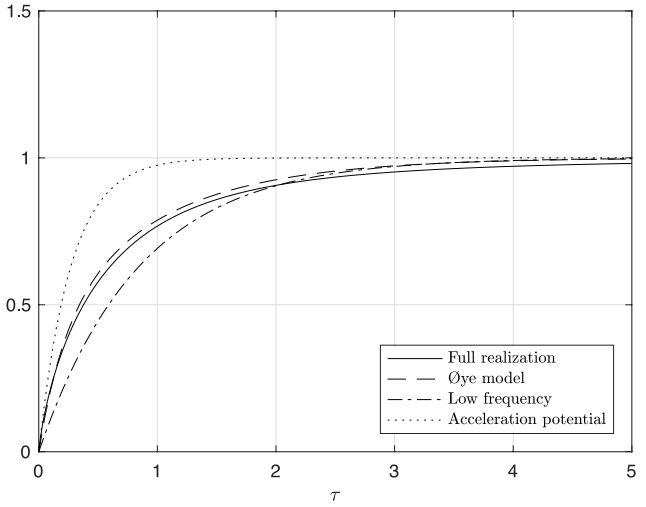

Figure 3.6: The low frequency model approximation model given in [2].

3.2.5 Validation of the aerodynamic model

In this section, the nonlinear aerodynamic model is tested and validated against reference models. Since most of the reference models available in the literature don't have an expression for the aerodynamic forces in six degrees of freedom, a sub-model of the derived system is used to validate against available models. The reduced model used is shown in equation 3.63. In this case, the NREL 5MW reference rotor [14] has been implemented for the test of the model. The rotor specification is discussed in detail in chapter 5. A set of velocities were tested and compared against data determined by a BEM model presented in [2].

$$\boldsymbol{\tau}_{\mathrm{hyd},(1,4)} = \rho B \left[\bar{\boldsymbol{\Lambda}}_{(1,4)} + \alpha_0 \boldsymbol{\Lambda}_{0,(1,4)}) + \bar{\boldsymbol{\Delta}}_{(1,4)} \right] \boldsymbol{\mu} \tag{3.63}$$

where the subscript 1,4 represent the thrust in x axis and the torque about x axis. The sub matrices of the model are defined as

$$\bar{\boldsymbol{\Lambda}}_{(1,4)} = \begin{bmatrix} 0 & c_1\mu_1 - \mu_4 s_2 \\ \mu_4 s_2 - c_1\mu_1 & 0 \end{bmatrix},$$

$$\boldsymbol{\Lambda}_{0,(1,4)} = \begin{bmatrix} 0 & -c_2\mu_4 - \mu_1 s_1 \\ c_2\mu_4 + \mu_1 s_1 & 0 \end{bmatrix}, \bar{\boldsymbol{\Delta}}_{(1,4)} = \begin{bmatrix} a_0 & 0 \\ 0 & a_2 \end{bmatrix} \tag{3.64}$$

Wind Speed (m/s)	Thrust (model)(kN)	Power (model) (MW)	Thrust (BEM) (kN)	Power (BEM) (MW)	Thrust Errors (%)	Power Errors (%)
5.0	160	0.47	180	0.44	15.60	3.88
6.0	222	0.81	260	0.78	12.92	8.01
7.0	300	1.29	360	1.24	9.94	6.92
8.0	390	1.93	420	1.92	7.31	4.25
9.0	500	2.70	570	2.68	5.08	4.37
10.0	590	3.7	600	3.6	2.01	4.42
11.4	710	5.2	730	5.17	3.91	0.73

Table 3.1: Simulation values from the modeled system compared against simulation done in [2]

As shown in the table 3.1, the steady state simulation for the tested set of velocities shows an excellent result compared to the BEM data. Further, for the wind velocity greater than 11.4 (the rated speed), the model has been tested using a pitch controller. The pitch controller is used to keep the power at the rated power. The mean objective of simulating the controlled system in this case is to validate the blade pitch modeling. The controlled thrust and power curves are shown in figure 3.7.

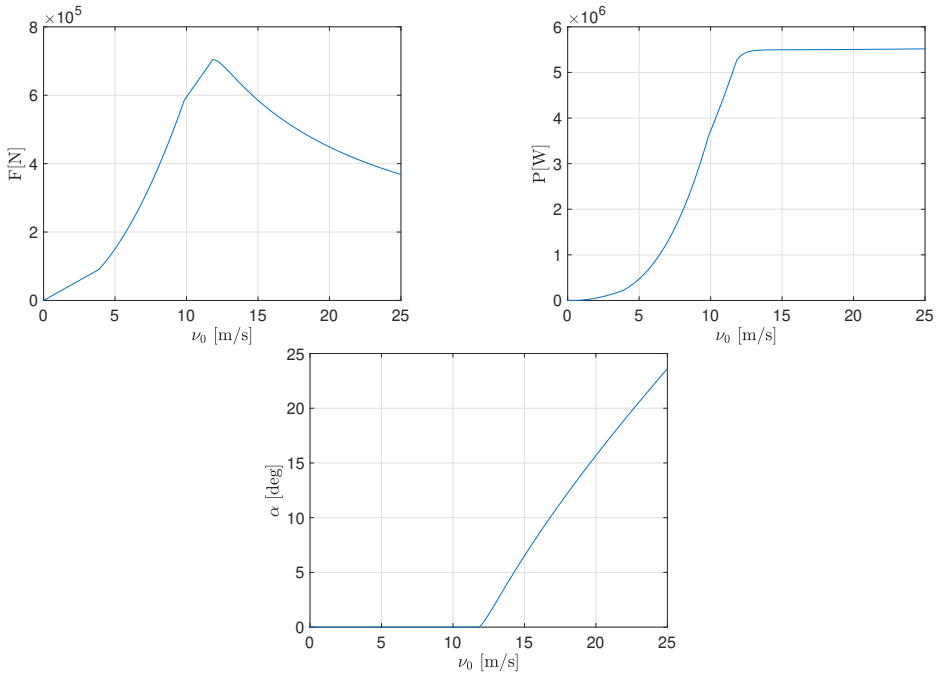

Figure 3.7: Steady state thrust and power curve and collective pitch angle as a function of wind speed

3.3 Dynamic model of the rotor

The equation of motion for the rotor is derived in a similar approach as that for modeling of turbine platform. The equation may be summarized as

$$\boldsymbol{M}_r\dot{\boldsymbol{\nu}} + \boldsymbol{C}_r(\boldsymbol{\nu})\boldsymbol{\nu} = \boldsymbol{\tau}_{aer} - \tau_{gen} \tag{3.65}$$

$$\Updownarrow$$

$$\begin{bmatrix} m_r\mathbf{I}_{3\times3} & \mathbf{0}_{3\times3} \\ \mathbf{0}_{3\times3} & \mathbf{I}_r \end{bmatrix} \begin{bmatrix} \dot{\mathbf{v}}_{ir}^r \\ \dot{\omega}_{ir}^r \end{bmatrix} + \begin{bmatrix} m_r S(\omega_{ir}^r) & \mathbf{0}_{3\times3} \\ \mathbf{0}_{3\times3} & -S(\mathbf{I}_r\omega_{ir}^r) \end{bmatrix} \begin{bmatrix} \mathbf{v}_{ir}^r \\ \omega_{ir}^r \end{bmatrix} = \begin{bmatrix} \mathbf{f}^r \\ \mathbf{m}^r \end{bmatrix} \tag{3.66}$$

Here m_r is the rotor mass, $\mathbf{I}_r$ is the inertia tensor of the rotor and τ_{gen} is the generator torque. The generator torque is defined with the relation

$$I_{r,x}\dot{\Omega} = \mathbf{e}_\phi^\top \boldsymbol{\tau}_{aer} - \tau_{gen} \tag{3.67}$$

Here Ω is the rotation speed of the rotor and $\mathbf{e}_\phi$ is a selection vector defined such that

$$\mathbf{e}_\phi \triangleq \begin{bmatrix} 0 & 0 & 0 & 1 & 0 & 0 \end{bmatrix}^\top$$

Finally the equation derived in this chapter are summarized by

Aerodynamic force:

$$\boldsymbol{\tau}_{\text{aer}} = \boldsymbol{\tau}_{\text{lift}} + \boldsymbol{\tau}_{\text{drag}} = \rho B \left[\bar{\boldsymbol{\Lambda}}(\boldsymbol{\mu}) + \alpha_0 \boldsymbol{\Lambda}_0(\boldsymbol{\mu}) + \alpha_c \boldsymbol{\Lambda}_c(\boldsymbol{\mu}) + \alpha_s \boldsymbol{\Lambda}_s(\boldsymbol{\mu}) + \bar{\boldsymbol{\Delta}} \right] \boldsymbol{\mu} \tag{3.68}$$

Induced flow

$$2\rho A R \mu \dot{v}_i + 2\rho A |\mu_1| v_i = e_x^\top \boldsymbol{\tau}_{\text{aer}} \tag{3.69}$$

Generator equation

$$I_x^R \dot{\Omega} = \mathbf{e}_\phi^\top \boldsymbol{\tau}_{aer} - \tau_{gen} \tag{3.70}$$

Rotor equation

$$\boldsymbol{M}_r\dot{\boldsymbol{\nu}}^r + \boldsymbol{C}_r(\boldsymbol{\nu}^r)\boldsymbol{\nu}^r = \boldsymbol{\tau}_{aer} - \tau_{gen} \tag{3.71}$$

Chapter 4

Integrated state-space model

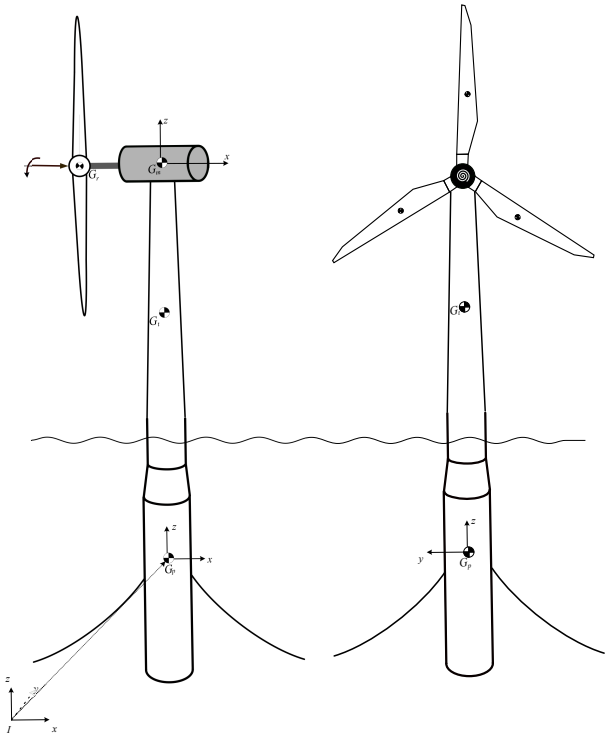

Figure 4.1: The floating win turbine geometri

In this chapter, the modeled platform in chapter 2 and the modeled rotor are integrated and presented as a linear state space model.

4.1 System integration

To sum up the platform and rotor model, some transformation has to be done. Now that the platform and the rotor are coordinate systems are coincident when the rotor is still, the relation between the generalized velocities can be expressed as:

$$\boldsymbol{\nu}^r = \boldsymbol{\nu}^p + e_\phi \Omega \tag{4.1}$$

The rotor equation of motion can then be expressed as

$$\boldsymbol{M}_r(\dot{\boldsymbol{\nu}}^p + e_\phi \dot{\Omega}) + \boldsymbol{C}_r(\boldsymbol{\nu}^p + e_\phi \Omega) = \boldsymbol{\tau}_{aer} - \tau_{gen} \tag{4.2}$$

By subtracting the generator equation, the rotor system are described by the two equation

$$\begin{aligned} \boldsymbol{M}_r \dot{\boldsymbol{\nu}}^p + \boldsymbol{C}_{rB}(\boldsymbol{\nu}^r)\boldsymbol{\nu} &= \boldsymbol{\tau}_{aer} - \mathbf{e}_\phi \mathbf{e}_\phi^\top \boldsymbol{\tau}_{aer} \\ &= \underbrace{\left(\mathbf{I}_{6\times 6} - \mathbf{e}_\phi \mathbf{e}_\phi^\top\right)}_{\triangleq \mathbf{K}} \boldsymbol{\tau}_{aer} \end{aligned} \tag{4.3}$$

$$I_x^R \dot{\Omega} = \mathbf{e}_\phi^\top \boldsymbol{\tau}_{aer} - \tau_{gen} \tag{4.4}$$

That allows us to summarize the rotor and platform equation of motion as shown in equation

$$(\boldsymbol{M}_p + \boldsymbol{M}_r + \boldsymbol{A})\dot{\boldsymbol{\nu}}^p + (\boldsymbol{C}_p + \boldsymbol{C}_r)\boldsymbol{\nu}^r + \boldsymbol{G}\boldsymbol{\eta} = \boldsymbol{\tau}_{hyd*} + \mathbf{K}\boldsymbol{\tau}_{aer} \tag{4.5}$$

4.2 State space formulation

It is not convenient to perform the control analysis of the system directly in the form of equation 4.5. It is preferable to transform the model into a state space model. A state space model can be written in the standard form

$$\dot{\mathbf{x}} = \mathbf{Ax+Bu} \tag{4.6}$$

$$\mathbf{y} = \mathbf{Cx+Du} \tag{4.7}$$

where **x** is a vector of the states, **u** is the inputs and **y** is a vector of outputs. States and inputs vectors for the turbine analysis is chosen such that:

$$\mathbf{x} = \begin{bmatrix} \boldsymbol{\eta} & \boldsymbol{\nu} & v_i & \Omega \end{bmatrix}^\top \tag{4.8}$$

$$\mathbf{u} = \begin{bmatrix} \alpha_0 & \alpha_s & \alpha_c & \tau_{gen} \end{bmatrix}^\top \tag{4.9}$$

4.2.1 Linearization of the dynamic equation

The dynamic system derived in equation 4.5 is a second-order nonlinear system, where the coriolis, lift, and drag forces depend on the velocity squared. As mentioned earlier in the report, the main target is to derive a linear state-space model equation for linear control development. In this section, the equation of motion is linearized about an operating point; the resulting linear model defines the system's dynamic behavior about the specific operating point. The linear system is then expressed as function of the perturbed states and input such as

$$\frac{d}{dt}(\boldsymbol{x}-\boldsymbol{x}_0) = \left.\frac{\partial f}{\partial x}\right|_{x_0,u_0}(\boldsymbol{x}-\boldsymbol{x}_0) + \left.\frac{\partial f}{\partial u}\right|_{x_0,u_0}(\boldsymbol{u}-\boldsymbol{u}_0) \tag{4.10}$$

$$= \bar{\boldsymbol{A}}\delta\boldsymbol{x} + \bar{\boldsymbol{B}}\delta\boldsymbol{u} \tag{4.11}$$

Equilibrium Point: The operating points are chosen such that the system in equilibrium,the system desired equilibrium points are obtained by solving the following equations:

$$\boldsymbol{\nu}_o = 0\ , \dot{\boldsymbol{\nu}}_o = 0, \dot{\boldsymbol{\Omega}}_o = 0,\ \dot{\boldsymbol{\nu}}_i = 0 \tag{4.12}$$

$$\begin{aligned}
0 &= -\mathbf{G}\boldsymbol{\eta}_o + \mathbf{K}\boldsymbol{\tau}_{aer,o} && \longrightarrow \boldsymbol{\eta}_o = \mathbf{G}^{-1}\mathbf{K}\boldsymbol{\tau}_{aer,o}\\
0 &= \mathbf{e}_\phi^\top\boldsymbol{\tau}_{aer,o} - \tau_{gen,o} && \longrightarrow \tau_{gen,o} = e_\phi^\top\boldsymbol{\tau}_{aer,o}\\
0 &= \mathbf{e}_x^\top\boldsymbol{\tau}_{\mathrm{aer,o}} - 2\rho A|\mu_{1,o}|v_{i,o} && \longrightarrow v_{i,o} = \frac{\mathbf{e}_x^\top\boldsymbol{\tau}_{\mathrm{aer,o}}}{2\rho A|\mu_{1,o}|}
\end{aligned}$$

Linearization of coriolis matrix:

$$C(\boldsymbol{\nu})\boldsymbol{\nu} = \begin{bmatrix} m_r S(\omega_{ir}^r) & \mathbf{0}_{3\times3} \\ \mathbf{0}_{3\times3} & -S(\mathbf{I}_r\omega_{ir}^r) \end{bmatrix}\begin{bmatrix} \mathbf{v}_{ig_r}^r \\ \omega_{ir}^r \end{bmatrix}$$

$$\begin{aligned}
C(\boldsymbol{\nu})\boldsymbol{\nu} &\approx C(\boldsymbol{\nu}_o)\boldsymbol{\nu}_o + \left.\frac{\partial C(\boldsymbol{\nu})\boldsymbol{\nu}}{\partial x}\right|_{\nu_o}\delta\boldsymbol{\nu}\\
&= C(\Omega_o)\delta\boldsymbol{\nu}
\end{aligned} \tag{4.13}$$

Here, the remaining term is the gyroscopic moment caused by the rotor spin. It is described as

$$\begin{bmatrix} 0 & 0 & 0 \\ 0 & 0 & I_{r,x}\Omega_o \\ 0 & -I_{r,x}\Omega_o & 0 \end{bmatrix}\begin{bmatrix} \delta\dot{\phi} \\ \delta\dot{\theta} \\ \delta\dot{\psi} \end{bmatrix} \tag{4.14}$$

Linearization of lift matrices

$$\boldsymbol{\tau}_{\text{lift}} \approx B\left[\bar{\boldsymbol{\Lambda}}(\boldsymbol{\mu}) + \alpha_0\boldsymbol{\Lambda}_0(\boldsymbol{\mu}) + \alpha_c\boldsymbol{\Lambda}_c(\boldsymbol{\mu}) + \alpha_s\boldsymbol{\Lambda}_s(\boldsymbol{\mu})\right]\boldsymbol{\mu} \tag{4.15}$$

$$\bar{\boldsymbol{\Lambda}}(\boldsymbol{\mu})\boldsymbol{\mu} \approx \bar{\boldsymbol{\Lambda}}(\boldsymbol{\mu}_0)\boldsymbol{\mu}_o + \left.\frac{\partial\bar{\boldsymbol{\Lambda}}(\boldsymbol{\mu})\boldsymbol{\mu}}{\partial\mu}\right|_{\boldsymbol{\mu}_o}\delta\boldsymbol{\mu} \tag{4.16}$$

Where $\boldsymbol{\mu}_o = \begin{bmatrix}\mu_{1,o} & 0 & 0 & \mu_{4,o} & 0 & 0\end{bmatrix}^\top$, that gives the matrices

$$\bar{\boldsymbol{\Lambda}}(\boldsymbol{\mu}_o)\boldsymbol{\mu}_o = \begin{bmatrix}(c_1\mu_{1,o} - \mu_{4,o}s_2)\mu_{4,o} & 0 & 0 & (\mu_{4,o}s_2 - c_1\mu_{1,o})\mu_{1,o} & 0 & 0\end{bmatrix}^\top \tag{4.17}$$

$$\left.\frac{\partial\bar{\boldsymbol{\Lambda}}(\boldsymbol{\mu})\boldsymbol{\mu}}{\partial\mu}\right|_{\boldsymbol{\mu}_o} = \underbrace{\begin{bmatrix} c_1\bar{\mu_4} & 0 & 0 & c_1\mu_{1,o}-2\mu_{4,o}s_2 & 0 & 0 \\ 0 & \frac{\bar{\mu_1}S_0}{2} & 0 & 0 & \frac{1}{2}(2c_1\mu_{1,o}-\mu_{4,o}s_2) & 0 \\ 0 & 0 & \frac{\bar{\mu_1}S_0}{2} & 0 & 0 & \frac{1}{2}(2c_1\mu_{1,o}-\mu_{4,o}s_2) \\ \mu_{4,o}s_2-2c_1\mu_{1,o} & 0 & 0 & \bar{\mu_1}s_2 & 0 & 0 \\ 0 & \frac{1}{2}(2\mu_{4,o}s_2-c_1\mu_{1,o}) & 0 & 0 & \frac{c_3\bar{\mu_4}}{2} & 0 \\ 0 & 0 & \frac{1}{2}(2\mu_{4,o}s_2-c_1\mu_{1,o}) & 0 & 0 & \frac{c_3\bar{\mu_4}}{2} \end{bmatrix}}_{\triangleq\bar{\boldsymbol{\Lambda}}_x} \tag{4.18}$$

By assuming small perturbation for velocities and pitch angle,
the term $\left[\alpha_0\boldsymbol{\Lambda}_0(\boldsymbol{\mu}) + \alpha_c\boldsymbol{\Lambda}_c(\boldsymbol{\mu}) + \alpha_s\boldsymbol{\Lambda}_s(\boldsymbol{\mu})\right]\boldsymbol{\mu}$ can simply be linearized to

$$= \underbrace{\begin{bmatrix} -\mu_{4,o}\left(\mu_{4,o}c_2 + \mu_{1,o}s_1\right) & 0 & 0 \\ 0 & -\frac{1}{2}\mu_{1,o}\left(\mu_{4,o}c_1 + \mu_{1,o}s_0\right) & 0 \\ 0 & 0 & \frac{1}{2}\mu_{1,o}\left(\mu_{4,o}c_1 + \mu_{1,o}s_0\right) \\ \mu_{1,o}\left(\mu_{4,o}c_2 + \mu_{1,o}s_1\right) & 0 & 0 \\ 0 & -\frac{1}{2}\mu_{4,o}\left(\mu_{4,o}c_3 + \mu_{1,o}s_2\right) & 0 \\ 0 & 0 & \frac{1}{2}\mu_{4,o}\left(\mu_{4,o}c_3 + \mu_{1,o}s_2\right) \end{bmatrix}}_{\triangleq\bar{\boldsymbol{\Lambda}}_u} \begin{bmatrix}\delta\alpha_0 \\ \delta\alpha_s \\ \delta\alpha_c\end{bmatrix} \tag{4.19}$$

The linearized lift is then expressed as

$$\boldsymbol{\tau}_{\text{lift}} \approx \rho B\left[\bar{\boldsymbol{\Lambda}}_o + \bar{\boldsymbol{\Lambda}}_x\delta\boldsymbol{\mu} + \bar{\boldsymbol{\Lambda}}_u\delta\boldsymbol{\alpha}\right] \tag{4.20}$$

Linearization of drag matrix:

$$\bar{\mathbf{\Delta}}(\tilde{\boldsymbol{\mu}})\boldsymbol{\mu} = \begin{bmatrix} a_0 & 0 & 0 & 0 & 0 & 0 \\ 0 & \frac{a_0}{2} & 0 & 0 & 0 & 0 \\ 0 & 0 & \frac{a_0}{2} & 0 & 0 & 0 \\ 0 & 0 & 0 & a_2 & 0 & 0 \\ 0 & 0 & 0 & 0 & \frac{a_2}{2} & 0 \\ 0 & 0 & 0 & 0 & 0 & \frac{a_2}{2} \end{bmatrix} \boldsymbol{\mu} \tag{4.21}$$

$$a_0 = d|\tilde{\boldsymbol{\mu}}| \int_0^R c(r)\sqrt{1+\left(\frac{r}{R}\right)^2}dr, a_2 = d|\tilde{\boldsymbol{\mu}}| \int_0^R c(r)r^2\sqrt{1+\left(\frac{r}{R}\right)^2}dr \tag{4.22}$$

$$\bar{\mathbf{\Delta}}(\tilde{\boldsymbol{\mu}})\boldsymbol{\mu} \approx \bar{\mathbf{\Delta}}(\tilde{\boldsymbol{\mu}}_o)\boldsymbol{\mu}_o + \frac{\partial}{\partial \boldsymbol{\mu}}\bar{\mathbf{\Delta}}(\tilde{\boldsymbol{\mu}})\mu\Big|_{\boldsymbol{\mu}=\boldsymbol{\mu}_o} \ \delta\boldsymbol{\mu} \tag{4.23}$$

$$\bar{\mathbf{\Delta}}(\tilde{\boldsymbol{\mu}})\boldsymbol{\mu} = |\tilde{\boldsymbol{\mu}}_o| \begin{bmatrix} a_0'\mu_{o,1} \\ 0 \\ 0 \\ a_2'\mu_{o,4} \\ 0 \\ 0 \end{bmatrix} + \underbrace{\frac{1}{|\tilde{\boldsymbol{\mu}}_o|} \begin{bmatrix} a_0'(2\mu_{o,1}^2 + R^2\mu_{o,4}^2) & 0 & 0 & a_0'(R^2\mu_{o,4}\mu_{o,1}) & 0 & 0 \\ 0 & \frac{a_0'}{2}|\tilde{\boldsymbol{\mu}}_o|^2 & 0 & 0 & 0 & 0 \\ 0 & 0 & \frac{a_0'}{2}|\tilde{\boldsymbol{\mu}}_o|^2 & 0 & 0 & 0 \\ a_2'(\mu_{o,4}\mu_{o,1}) & 0 & 0 & a_2'(2R^2\mu_{o,4}^2 + \mu_{o,1}^2) & 0 & 0 \\ 0 & 0 & 0 & 0 & \frac{a_2'}{2}|\tilde{\boldsymbol{\mu}}_o|^2 & 0 \\ 0 & 0 & 0 & 0 & 0 & \frac{a_2'}{2}|\tilde{\boldsymbol{\mu}}_o|^2 \end{bmatrix}}_{\triangleq \bar{\mathbf{\Delta}}_x} \delta\boldsymbol{\mu} \tag{4.24}$$

$a_0' = \frac{a_0}{|\tilde{\boldsymbol{\mu}}|} = d\int_0^R c(r)\sqrt{1+\left(\frac{r}{R}\right)^2}dr, a_2' = \frac{a_0}{|\tilde{\boldsymbol{\mu}}|} = d\int_0^R c(r)r^2\sqrt{1+\left(\frac{r}{R}\right)^2}dr$ The

linearized drag is then expressed as

$$\boldsymbol{\tau}_{\text{drag}} \approx \rho B\left[\bar{\mathbf{\Delta}}_o + \bar{\mathbf{\Delta}}_x\delta\boldsymbol{\mu}\right] \tag{4.25}$$

Linearization of the induced flow

$$\dot{v}_i = \frac{\mathbf{e}_x^\top \boldsymbol{\tau}_{\text{aer}}}{2\rho AR\mu} - \frac{2\rho A|\mu_1|v_i}{R\mu} \tag{4.26}$$

$$\delta\dot{v}_i = -\frac{2\rho A|\mu_{o,1}|}{R\mu}\ \delta v_i - \frac{2\rho A\mu_{o,1}\bar{v}_i}{R\mu|\mu_{o,1}|}\ \delta\mu_1 + \frac{\mathbf{e}_x^\top}{2\rho AR\mu}\ \delta\boldsymbol{\tau}_{\text{aer}} \tag{4.27}$$

Finally, the relative velocities are expanded by equation

$$\delta\boldsymbol{\mu} = \delta\boldsymbol{\nu}_0 - \delta\boldsymbol{\nu} - \delta\boldsymbol{e}_\phi\Omega - \delta\boldsymbol{\nu}_i \tag{4.28}$$

and the system can be summarized in a linear state space form

$$= \bar{\boldsymbol{A}}\delta\boldsymbol{x} + \bar{\boldsymbol{B}}\delta\boldsymbol{u} + \bar{\boldsymbol{E}}\delta\boldsymbol{\nu}_0$$

$$\begin{bmatrix} \delta\boldsymbol{\nu} \\ \delta\dot{\boldsymbol{\nu}} \\ \delta\dot{v}_i \\ \delta\dot{\Omega} \end{bmatrix} = \begin{bmatrix} \mathbf{0}_{6\times6} & \mathbf{I}_{6\times6} & \mathbf{0}_{6\times1} & \mathbf{0}_{6\times1} \\ -\mathbf{M}^{-1}\mathbf{G} & -\mathbf{M}^{-1}\mathbf{C}-\mathbf{M}^{-1}\mathbf{K}(\bar{\boldsymbol{\Lambda}}_x+\bar{\boldsymbol{\Delta}}_x) & -\mathbf{M}^{-1}\mathbf{K}(\bar{\boldsymbol{\Lambda}}_x+\bar{\boldsymbol{\Delta}}_x)\mathbf{e}_\phi & -\mathbf{M}^{-1}\mathbf{K}(\bar{\boldsymbol{\Lambda}}_x+\bar{\boldsymbol{\Delta}}_x)\mathbf{e}_x \\ \mathbf{0}_{1\times6} & -\mathbf{e}_x^\top(\bar{\boldsymbol{\Lambda}}_x+\bar{\boldsymbol{\Delta}}_x) & -\mathbf{e}_x^\top(\bar{\boldsymbol{\Lambda}}_x+\bar{\boldsymbol{\Delta}}_x)\mathbf{e}_\phi & -\mathbf{e}_x^\top(\bar{\boldsymbol{\Lambda}}_x+\bar{\boldsymbol{\Delta}}_x)\mathbf{e}_\phi \\ \mathbf{0}_{1\times6} & -(I_x^R)^{-1}\mathbf{e}_\phi^\top(\bar{\boldsymbol{\Lambda}}_x+\bar{\boldsymbol{\Delta}}_x) & -(I_x^R)^{-1}\mathbf{e}_\phi^\top(\bar{\boldsymbol{\Lambda}}_x+\bar{\boldsymbol{\Delta}}_x)\mathbf{e}_x & -(I_x^R)^{-1}\mathbf{e}_\phi^\top(\bar{\boldsymbol{\Lambda}}_x+\bar{\boldsymbol{\Delta}}_x)\mathbf{e}_\phi \end{bmatrix} \begin{bmatrix} \delta\boldsymbol{\eta} \\ \delta\boldsymbol{\nu} \\ \delta v_i \\ \delta\Omega \end{bmatrix}$$
$$+ \begin{bmatrix} \mathbf{0}_{6\times4} & \\ \mathbf{M}^{-1}\mathbf{K}\bar{\boldsymbol{\Lambda}}_u & 0 \\ \mathbf{e}_\phi^\top\bar{\boldsymbol{\Lambda}}_u & 0 \\ \frac{1}{2\rho AR\mu}\mathbf{e}_x^\top\bar{\boldsymbol{\Lambda}}_u & 1 \end{bmatrix} \begin{bmatrix} \delta\alpha_0 \\ \delta\alpha_s \\ \delta\alpha_c \\ \delta\tau_{gen} \end{bmatrix} + \begin{bmatrix} \mathbf{0}_{6\times6} \\ \mathbf{M}^{-1}\mathbf{K}(\bar{\boldsymbol{\Lambda}}_x + \bar{\boldsymbol{\Delta}}_x) \\ (I_x^R)^{-1}\mathbf{e}_\phi^\top(\bar{\boldsymbol{\Lambda}}_x + \bar{\boldsymbol{\Delta}}_x) \\ \mathbf{e}_x^\top(\bar{\boldsymbol{\Lambda}}_x + \bar{\boldsymbol{\Delta}}_x) \end{bmatrix} \delta\boldsymbol{\nu}_0 \tag{4.29}$$

Chapter 5

Model Validation and simulation

5.1 OC3-Hywind

The validations analysis is based on the horizontal axis 5MW reference wind turbine, designed by National Renewable Energy Laboratory(NREL). The specification for the turbine is based on NREL published results. The turbine dimensions and specifications are presented in Table 5.1.

Parameter	**Value**
-Water Depth	320 m
-Draft	120 m
-Water displacement	8029 m
-Tower height over water level	90 m
-Mass, including ballast	7 466 000 kg
-Center of gravity location of the platform below still water level	89.92 m
-Pitch inertia about center of gravity	4229000000 kg/m^2
-Depth to fairleads, anchors	70 m
-Center of buoyancy,location of the platform below still water level	62.06 m
-Metacentric hight GM, above the center of mass	27.86 m
-Mooring stiffness veritcal direction	11940 N/m
-Mooring stiffness horizontal direction	41180 N/m

Table 5.1: OC3-Hywind Platform Specifications

The values are gathered from the technical report *Definition of the Floating System for Phase IV of OC3*, by J. Jonkman[15] and the paper *Experimental Comparison of Three Floating Wind Turbine Concepts*[16].

NREL 5MW

The OC3 wind turbine rotor, is the NREL 5MW reference rotor

Node	RNnodes	Blade chord	Blade twist
1	2.8667	3.542	13.308
2	5.6000	3.854	13.308
3	8.3333	4.167	13.308
4	11.7500	4.557	13.308
5	15.8500	4.652	11.480
6	19.9500	4.458	10.162
7	24.0500	4.249	9.011
8	28.1500	4.007	7.795
9	32.2500	3.748	6.544
10	36.3500	3.502	5.361
11	40.4500	3.256	4.188
12	44.5500	3.010	3.125
13	48.6500	2.764	2.319
14	52.7500	2.518	1.526
15	56.1667	2.313	0.863
16	58.9000	2.313	0.370
17	61.6333	1.419	0.106

Table 5.2: NREL 5MW rotor specifications

5.2 Numerical simulation

The developed linear state space model is implemented in `MATLAB` [17] for numerical simulation. The simulation result is used to validate the model against simulation data developed with numerical tools FAST and HAWAC2 [6][7]. Several load cases are defined in [3] for system validation. Two load cases are used to validate defined in table **??** the model against data in [3].

Load case (LC)	Wind condition	Wave condition	Analysis type
1.2	None	None (still water)	Eigen frequencies
1.4	None	None (still water)	Free decay test

Table 5.3: Load cases specified in [3]

5.2.1 Load Case 1.2

As described in the table above, in this load case, the wind and wave loads are set to zero to examine the system's eigen frequencies. The result of the simulation is shown in figure 5.1. The eigen frequencies predicted by the model are higher than the other simulation codes but lie in a reasonable range. The deviations are not unexpected and could be attributed to the different modeling techniques used to model the turbine and the linearization.

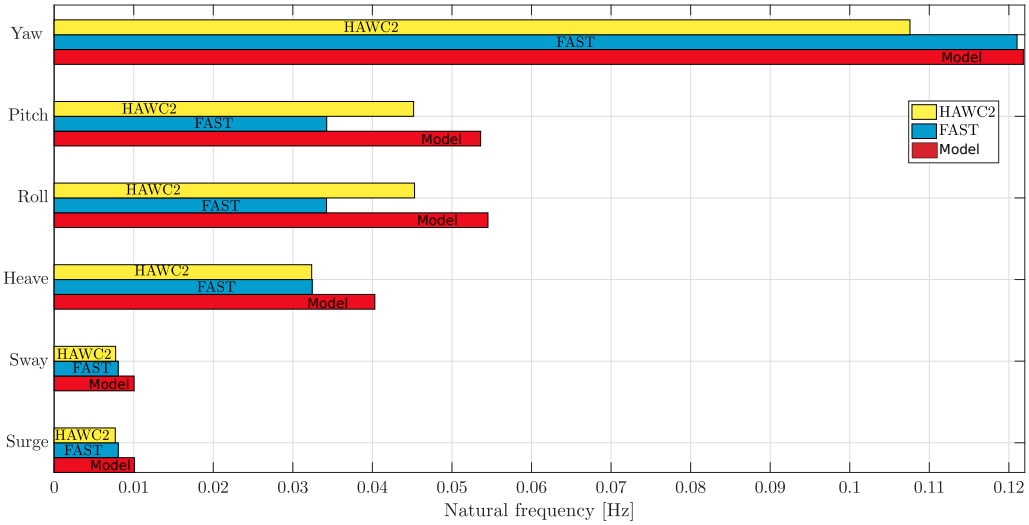

Figure 5.1: System natural frequencies

5.2.2 Load Case 1.4

Load case 1.4 is called free decay test and describes the platform behavior after starting in some non equilibrium points. The aerodynamic and wave loads are zero in this case also, the test case shows if the elements such as hydrostatic, hydrodynamic and mooring forces are modeled correctly. The result of the simulation in surge and Heave are in the same range as the given data, while the pitch seems to have a slower convergence. That may be explained by the neglected effect of radiation damping in the modeling. The results are illustrated in figure 5.2

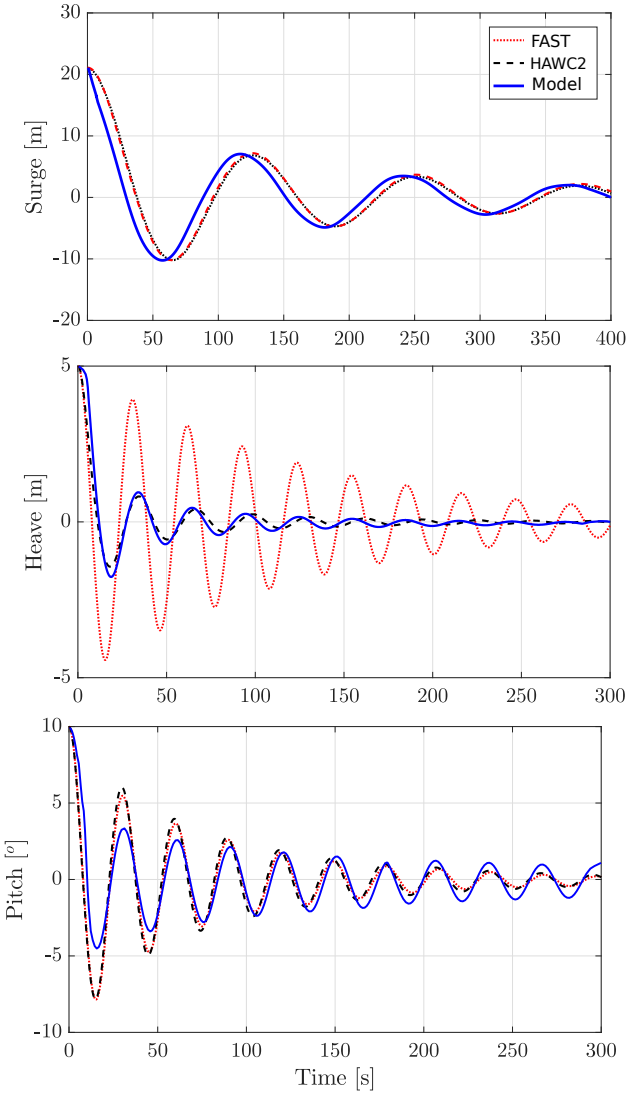

Figure 5.2: System Free decay test

The result in plots combines the modeled system simulation, the data plots from in [18]

5.3 Controllablity validation

The modeled linear state space system has four control inputs to the system, generator torque, collective pitch, and cyclic pitch angles. It is important to examine if the control inputs enough to control the system. One of the methods that can be used to examine the system controllability is the PBH test, which is used in this case.

PBH Test:

(A, B) is controllable if and only if $\mathrm{Rank}[A - \lambda I \quad B] = n$ for all eigenvalues λ of A[19].

Examining the PBH test show that the system is controllable using the four control input.

Chapter 6

Conclusion and further work

6.1 Conclusion

A 7-DOF rigid body dynamic model was developed to analyze the dynamics for use in developing a control system. The model considered hydrodynamic, hydrostatic, and mooring forces for the platform and focused on deriving a new aerodynamic model mainly based on the Kutta Jouski lifting theory.

The integration of the forces over the rotor blade length was expressed explicitly in different geometrical integral parameters. That approach of derivation included a lot of complicated mathematical calculations compared to the most used method BEMT. However, the resulted model is simple to implement, where most of the calculations are predetermined in these geometrical parameters. The derived aerodynamic was represented in vectroial form, that express the collective and cyclic blade pitch forces in six DOF, and was validated against experimental data.

Finally, the complete model of the floating wind turbine has been presented in the simple and well known state space form. The state space model is one of the most used forms in control development, and it is easy to implement. The model has 14 states, and four control inputs for the collective, cyclic pitch and the generator torque, the system controllability using those were tested by checking the PBH controllability criteria. Several simulation cases have been made to validate the system against experimental simulation with good agreements.

6.2 Further work

The derived model performed well in the analyses and simulation done in this work. However, the system is not tested in the development of a control strategy, which may be done as the next step for model validation.

As mentioned early in the report, the blade element method is the most used approach for aerodynamic modeling, augmentation of the nonuniform, and unsteady wind using this approach is a challenging task. However, the way that retaliative velocities described in the modeled aerodynamic in this work makes it possible to augment the nonuniform wind explicitly, while retaining the underlying structure of the model presented in this work. The augmentation of the nonuniform wind loads will be an improvement for the model and gives more realistic representation, this can be subject to further work on this topic.

Bibliography

[1] iea. International energy agency world energy outlook 2019. https://www.iea.org/weo2019/.

[2] Morten Dinhoff Pedersen. *Stabilization of Floating Wind Turbines*. NTNU, 2017.

[3] Jason Jonkman and Walter Musial. Offshore code comparison collaboration (oc3) for iea wind task 23 offshore wind technology and deployment. Technical report, National Renewable Energy Lab.(NREL), Golden, CO (United States), 2010.

[4] Morten D Pedersen and Thor I Fossen. Efficient nonlinear wind-turbine modeling for control applications. *IFAC Proceedings Volumes*, 45(2):264–269, 2012.

[5] Denis Matha, Markus Schlipf, Andrew Cordle, Ricardo Pereira, and Jason Jonkman. Challenges in simulation of aerodynamics, hydrodynamics, and mooring-line dynamics of floating offshore wind turbines. Technical report, National Renewable Energy Lab.(NREL), Golden, CO (United States), 2011.

[6] Jason M Jonkman, Marshall L Buhl Jr, et al. Fast user's guide. *Golden, CO: National Renewable Energy Laboratory*, 365:366, 2005.

[7] Torben J Larsen and Anders Melchior Hansen. How 2 hawc2, the user's manual. 2007.

[8] T.I. Fossen. *Handbook of Marine Craft Hydrodynamics and Motion Control*. John Wiley & Sons, 2011.

[9] Turgut Sarpkaya, Michael Isaacson, and JV Wehausen. Mechanics of wave forces on offshore structures. 1982.

[10] Odd Faltinsen. *Sea loads on ships and offshore structures*, volume 1. Cambridge university press, 1993.

[11] Roy Featherstone. *Rigid body dynamics algorithms*. Springer, 2014.

[12] Emmanuel Branlard. *Wind turbine aerodynamics and vorticity-based methods*, volume 10. Springer, 2017.

[13] Wayne Johnson. *Helicopter theory*. Courier Corporation, 2012.

[14] Jason Jonkman, Sandy Butterfield, Walter Musial, and George Scott. Definition of a 5-mw reference wind turbine for offshore system development. Technical report, National Renewable Energy Lab.(NREL), Golden, CO (United States), 2009.

[15] J. M. Jonkman. *"Definition of the Floating System for Phase IV of OC3",Tech. Rep. NREL/TP-500-47535*. National Renewable Energy Laboratory, 2010.

[16] Andrew J. Goupee, Bonjun J. Koo, Richard W. Kimball, Kostas F. Lambrakos, and Habib J. Dagher. Experimental Comparison of Three Floating Wind Turbine Concepts. *Journal of Offshore Mechanics and Arctic Engineering*, 136(2), 03 2014. 020906.

[17] MATLAB Version. 9.3. 0 (r2017b). *The MathWorks Inc, Natick, Massachusetts*, 2017.

[18] Mohammed Khair Al-Solihat, Meyer Nahon, and Kamran Behdinan. Dynamic modeling and simulation of a spar floating offshore wind turbine with consideration of the rotor speed variations. *Journal of Dynamic Systems, Measurement, and Control*, 141(8), 2019.

[19] Branislav Kisacanin and Gyan C Agarwal. *Linear Control Systems: with solved problems and MATLAB examples*. Springer Science & Business Media, 2012.

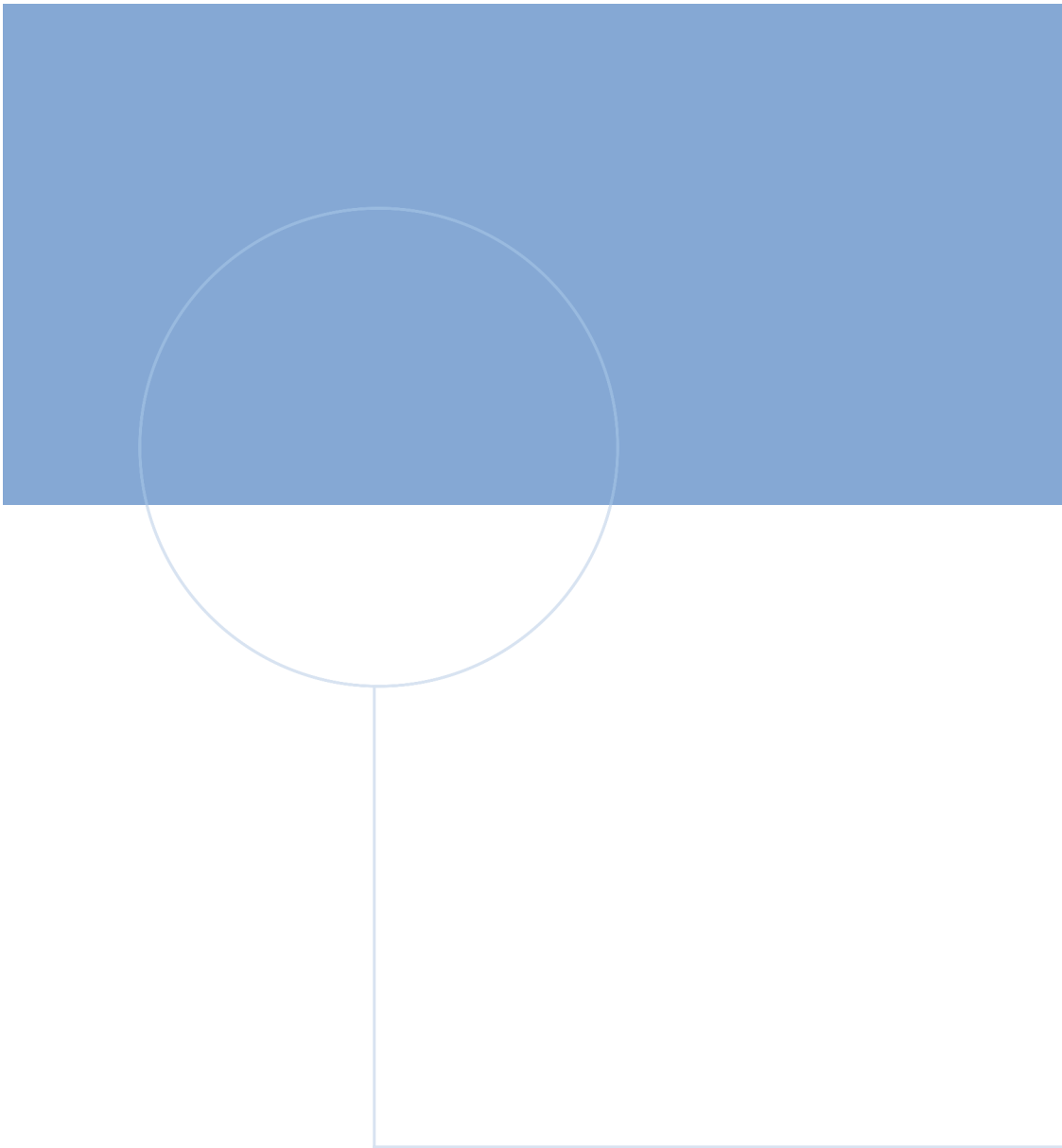

NTNU

Norwegian University of
Science and Technology